LETTERS
PUBLISHED ONLINE: 9 NOVEMBER 2015 | DOI: 10.1038/NMAT4463
nature materials

Tough bonding of hydrogels to diverse non-porous surfaces

Hyunwoo Yuk[1], Teng Zhang[1], Shaoting Lin[1], German Alberto Parada[1,2] and Xuanhe Zhao[1,3]*

In many animals, the bonding of tendon and cartilage to bone is extremely tough (for example, interfacial toughness ~800 J m^{-2}; refs 1,2), yet such tough interfaces have not been achieved between synthetic hydrogels and non-porous surfaces of engineered solids[3–9]. Here, we report a strategy to design tough transparent and conductive bonding of synthetic hydrogels containing 90% water to non-porous surfaces of diverse solids, including glass, silicon, ceramics, titanium and aluminium. The design strategy is to anchor the long-chain polymer networks of tough hydrogels covalently to non-porous solid surfaces, which can be achieved by the silanation of such surfaces. Compared with physical interactions, the chemical anchorage results in a higher intrinsic work of adhesion and in significant energy dissipation of bulk hydrogel during detachment, which lead to interfacial toughness values over 1,000 J m^{-2}. We also demonstrate applications of robust hydrogel–solid hybrids, including hydrogel superglues, mechanically protective hydrogel coatings, hydrogel joints for robotic structures and robust hydrogel–metal conductors.

Hybrid combinations of hydrogels and solid materials, including metals, ceramics, glass, silicon and polymers, are used in areas as diverse as biomedicine[10,11], adaptive and responsive materials[12], antifouling[13], actuators for optics[14] and fluidics[15], soft electronics[16] and machines[17]. Although hydrogels with extraordinary physical properties have been recently developed[3–9], the weak and brittle bonding between hydrogels and solid materials often severely hampers their integration and function in devices and systems. Whereas intense efforts have been devoted to the development of tough hydrogel–solid interfaces, previous works are generally limited to special cases with porous solid substrates[18]. Robust adhesion of dry elastomers to non-porous solids has been achieved[19–22], but such adhesion is not applicable to hydrogels that contain significant amounts of water[23]. The need for general strategies and practical methods for the design and fabrication of tough hydrogel bonding to diverse solid materials has remained a central challenge for the field.

Here, we report a design strategy and a set of simple fabrication methods to give extremely tough and functional bonding between hydrogels and diverse solids, including glass, silicon, ceramics, titanium and aluminium, to achieve interfacial toughness values over 1,000 J m^{-2}. The new design strategy and fabrication methods do not require porous or topographically patterned surfaces of the solids, and allow the hydrogels to contain over 90 wt% of water. The resultant tough bonding is also optically transparent and electrically conductive. In addition, we demonstrate novel functions of hydrogel–solid hybrids uniquely enabled by the tough bonding, including tough hydrogel superglues, hydrogel coatings that are mechanically protective, hydrogel joints for robotic structures and robust hydrogel–metal conductors. The design strategy and simple yet versatile method open new avenues not only to addressing fundamental questions on hydrogel–solid interfaces in biology, physics, chemistry and materials science, but also to practical applications of robust hydrogel–solid hybrids in diverse areas[10–17,24].

The proposed strategy to design tough hydrogel–solid bonding is illustrated in Fig. 1. As interfacial cracks can kink and propagate in relatively brittle hydrogel matrices (see Supplementary Movie 1, for example), the design of tough hydrogel–solid bonding first requires high fracture toughness of the constituent hydrogels[18]. Whereas tough hydrogels generally consist of covalently crosslinked long-chain polymer networks that are highly stretchable and other components that dissipate mechanical energy under deformation[25,26], it is impractical to chemically bond all components of the hydrogels on solid surfaces. We propose that it is sufficient to achieve relatively tough hydrogel–solid bonding by chemically anchoring the long-chain polymer network of a tough hydrogel on solid surfaces, as illustrated in Fig. 1a. When such a chemically anchored tough hydrogel is detached from a solid, the scission of the anchored layer of polymer chains gives the intrinsic work of adhesion Γ_0 (ref. 27; Fig. 1b). Meanwhile, the tough hydrogel around the interface will be highly deformed and thus dissipate a significant amount of mechanical energy[20–22,28], which further contributes to the interfacial toughness by Γ_D (Fig. 1b). Neglecting contributions from mechanical dissipation in the solid and friction on the interface, we can express the total interfacial toughness of the hydrogel–solid bonding as

$$\Gamma = \Gamma_0 + \Gamma_D \quad (1)$$

In equation (1), Γ_0 may be much lower than Γ_D for tough hydrogel–solid bonding, but it is still critical to chemically anchor long-chain polymer networks of tough hydrogels on the solids' surfaces. This is because the chemical anchorage gives a relatively high intrinsic work of adhesion Γ_0 (compared with physically attached cases), which maintains cohesion of the hydrogel–solid interface while allowing large deformation and mechanical dissipation to be developed in the bulk hydrogel to give high values of Γ_D (Fig. 1b).

To test the proposed design strategy, we use a functional silane, 3-(trimethoxysilyl) propyl methacrylate (TMSPMA), to modify the surfaces of glass, silicon wafer, titanium, aluminium and mica ceramic (Fig. 2a)[29]. We then covalently crosslink the long-chain polymer network of polyacrylamide (PAAm) or polyethylene glycol diacrylate (PEGDA) to the silanes on the modified surfaces of various solids. (See Methods and Supplementary Fig. 1a for details on the modification and anchoring process.) To form

[1]Soft Active Materials Laboratory, Department of Mechanical Engineering, Massachusetts Institute of Technology, Cambridge, Massachusetts 02139, USA. [2]Department of Chemical Engineering, Massachusetts Institute of Technology, Cambridge, Massachusetts 02139, USA. [3]Department of Civil and Environmental Engineering, Massachusetts Institute of Technology, Cambridge, Massachusetts 02139, USA. *e-mail: zhaox@mit.edu

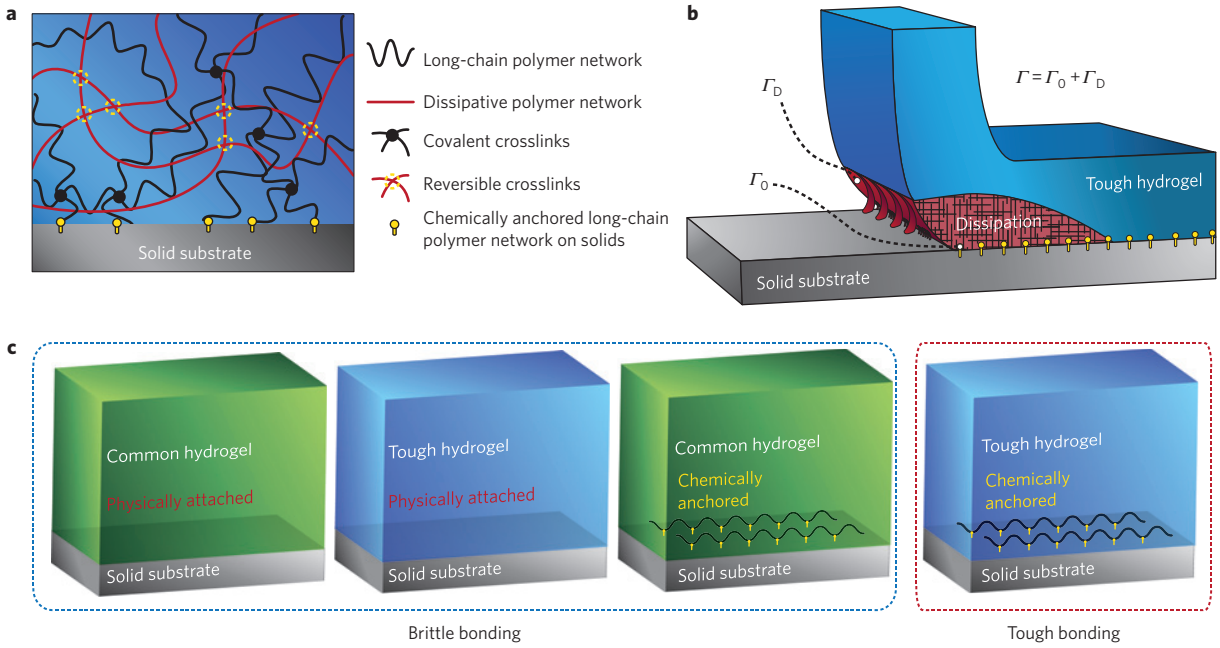

Figure 1 | A design strategy for tough bonding of hydrogels to diverse solids. a, The tough bonding first requires high fracture toughness of the constituent hydrogels. Whereas tough hydrogels generally consist of long-chain polymer networks and mechanically dissipative components, it is sufficient to achieve tough bonding by chemically anchoring the long-chain networks on solid surfaces. **b**, The chemical anchoring gives a relatively high intrinsic work of adhesion Γ_0, which maintains cohesion of the hydrogel–solid interface and allows large deformation and mechanical dissipation to be developed in the hydrogel during detachment. The dissipation further contributes to the total interfacial toughness by Γ_D. **c**, Schematics of various types of hydrogel–solid interfaces to be tested in the current study to validate the proposed design strategy (from left to right): common and tough hydrogels physically attached on solids, and common and tough hydrogels chemically anchored on solids.

tough hydrogels, the long-chain polymer network is interpenetrated with a reversibly crosslinked network of alginate, chitosan or hyaluronan[6,26], in which the reversible crosslinking and chain scission dissipate mechanical energy, as illustrated in Fig. 1a,b. (See Methods for details on the formula and procedures to make various hydrogels.) As control samples, we chemically anchor a pure PAAm or PEGDA hydrogel on silanized solid surfaces, and physically attach the pure PAAm or PEGDA hydrogel and corresponding tough hydrogels on untreated solid surfaces, as illustrated in Fig. 1c. The shear moduli of all hydrogels in the as-prepared states are set to be at the same level, ~30 kPa, by controlling the crosslinking densities in the hydrogels.

The samples of tough (for example, PAAm-alginate) and common (for example, PAAm) hydrogels chemically anchored and physically attached on glass substrates all look identical, as they are transparent with transmittance over 95%. We demonstrate the transparency of a sample in Fig. 2b by placing it above the 'MIT MECHE' colour logo. We then carry out a standard 90-degree peeling test with a peeling rate of 50 mm min^{-1} to measure the interfacial toughness between hydrogel sheets with a thickness of 3 mm and the glass substrates. A thin (~25 μm thick) and rigid glass film backing is attached to the other surface of the hydrogel sheet to prevent its elongation along the peeling direction. Thus, the measured interfacial toughness is equal to the steady-state peeling force per width of the hydrogel sheet[30]. (See Methods and Supplementary Fig. 2 for details of the peeling test.) Supplementary Movie 1 and Fig. 2c–e demonstrate the peeling process of the common hydrogel chemically anchored on the glass substrate. It can be seen that a crack initiates at the hydrogel–solid interface, kinks into the brittle hydrogel, and then propagates forward. The measured interfacial toughness is 24 J m^{-2} (Fig. 2i), limited by the hydrogel's fracture toughness, validating that tough hydrogels are indeed critical in the design of tough hydrogel–solid interfaces. Supplementary Movie 2 and Supplementary Fig. 3 demonstrate a typical peeling process of a tough or common hydrogel physically attached on the glass substrate. Different from the previous process shown in Supplementary Movie 1 and Fig. 2c–e, the crack can easily propagate along the interface without kinking or significantly deforming the hydrogel, giving a very low interfacial toughness of 8 J m^{-2} (Fig. 2i). Supplementary Movie 3 and Fig. 2f–h demonstrate the peeling process of the tough hydrogel with its long-chain network chemically anchored on the glass substrate. As the peeling force increases, the hydrogel around the interfacial crack front becomes highly deformed and subsequently unstable[31,32], developing a pattern of fingers before the interfacial crack can propagate. When the peeling force reaches a critical value, the crack begins to propagate along the hydrogel–solid interface (Fig. 2g). During crack propagation, the fingers coarsen with increasing amplitude and wavelength, and then detach from the substrate (Fig. 2h). The measured interfacial toughness is over 1,500 J m^{-2} (Fig. 2i), superior to natural counterparts such as tendon and cartilage on bones. As control cases, we vary the thickness of the tough hydrogel sheet from 1.5 mm to 6 mm, and obtain similar values of interfacial toughness (Supplementary Fig. 4). We further vary the peeling rate of the test from 200 mm min^{-1} to 5 mm min^{-1}, and find that the measured interfacial toughness decreases from 3,100 J m^{-2} to 1,500 J m^{-2} accordingly (Supplementary Fig. 5). It is evident that the measured interfacial toughness of chemically anchored PAAm-alginate hydrogel is rate-dependent, possibly owing to viscoelasticity of the hydrogel (Supplementary Fig. 5). Furthermore, the peeling rate used in the current study (50 mm min^{-1}) gives an interfacial toughness around the lower asymptote, which reflects the effects of intrinsic work of adhesion and rate-independent dissipation, such as the Mullins effect[33].

To understand the phenomena described above and the interfacial toughening mechanism, we develop a finite-element model to simulate the peeling process of a hydrogel sheet from a rigid substrate under a plane-strain condition. In the model, the intrinsic work of adhesion Γ_0 is characterized by a layer of cohesive elements

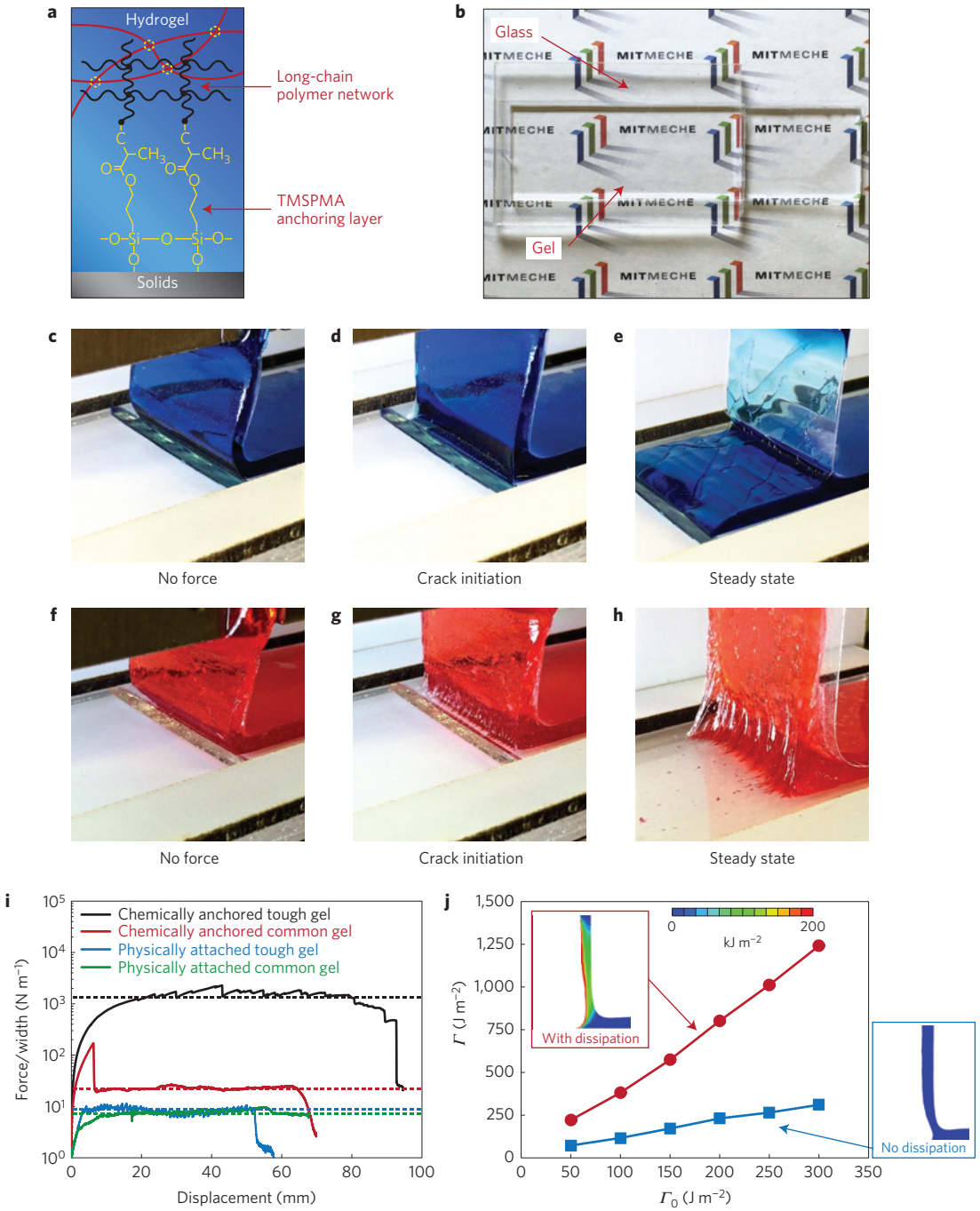

Figure 2 | Experimental and modelling results on various types of hydrogel–solid bonding. a, The chemical anchoring of long-chain polymer networks is achieved by crosslinking the networks to functional silanes grafted on the surfaces of various solids. **b**, The high transparency of the hydrogel–solid bonding is demonstrated by a colourful logo 'MIT MECHE' behind a hydrogel–glass hybrid. **c**–**e**, Photos of the peeling process of a common hydrogel chemically anchored on a glass substrate. **f**–**h**, Photos of the peeling process of a tough hydrogel with its long-chain network chemically anchored on a glass substrate. (Note that blue and red food dyes are added into the common and tough hydrogels, respectively, to enhance the contrast of the interfaces.) **i**, Curves of the peeling force per width of hydrogel sheet versus displacement for various types of hydrogel–solid bonding. **j**, Calculated interfacial fracture toughness Γ as a function of the prescribed intrinsic work of adhesion Γ_0 in finite-element models for the tough hydrogel (red line) and a pure elastic hydrogel with no mechanical dissipation but otherwise the same properties as the tough hydrogel (blue line). The contours in the inset figures indicate mechanical energy dissipated per unit area.

and the dissipative property of the PAAm-alginate hydrogel is characterized by the Mullins effect[33]. (See Supplementary Information and Supplementary Figs 13–19 and Supplementary Movies 8 and 9 for details of the model.) Figure 2j gives the calculated relation between the intrinsic work of adhesion Γ_0 and the interfacial toughness Γ. It is evident that the interfacial toughness increases monotonically with the intrinsic work of adhesion, which is effectively augmented by a factor determined by the dissipative properties of the hydrogel. We also vary the thickness of the tough hydrogel in the model from 0.8 to 6 mm and find that the calculated interfacial toughness is approximately the same, consistent with the experimental observation (Supplementary Figs 4 and 19). As a

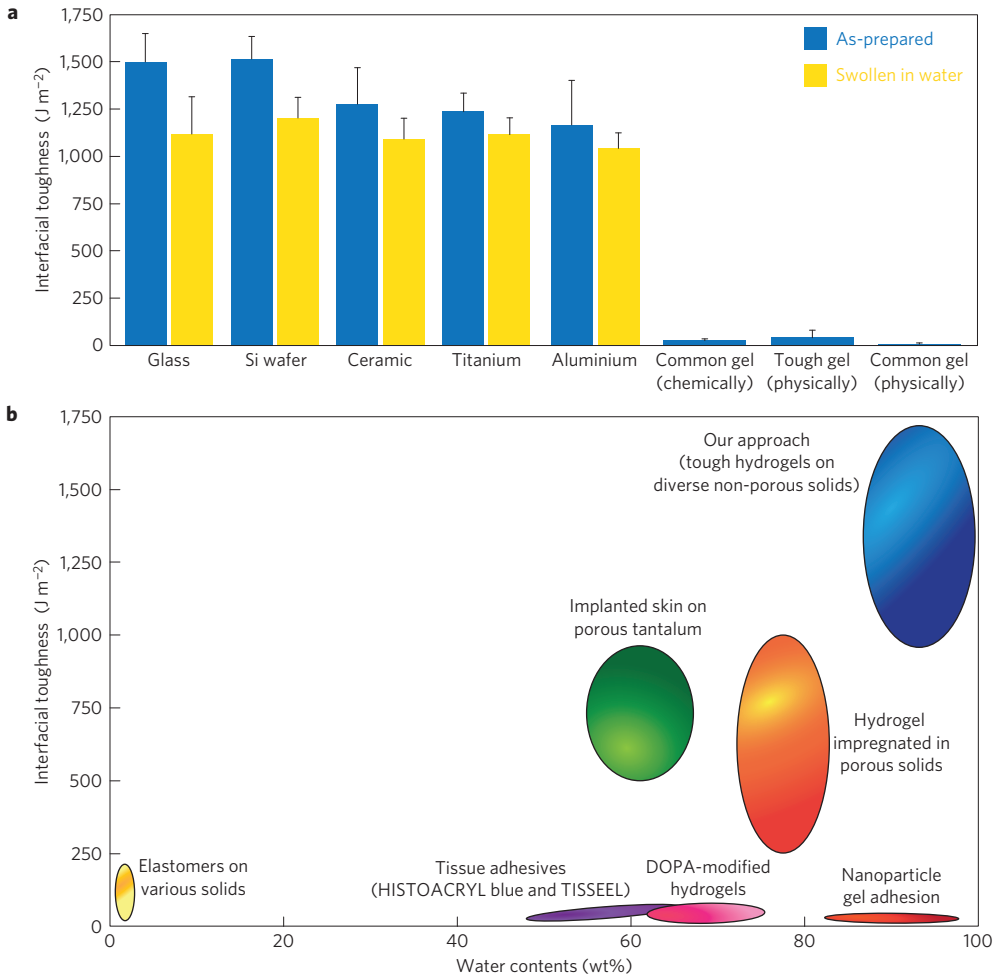

Figure 3 | Performance of the tough bonding of hydrogels to various solids. a, Measured interfacial toughness values of PAAm-alginate hydrogel bonded on glass, silicon wafer, ceramic, titanium and aluminium are consistently high, over 1,000 J m^{-2}, in both the as-prepared and swollen states. In contrast, the interfacial toughness values of the control samples are very low, 8–20 J m^{-2}, in the as-prepared state. (As the control samples debond from solids in the fully swollen state, the interfacial toughness is not measured.) **b**, Comparison of interfacial toughness of PAAm-alginate hydrogel bonded on diverse solids and other hydrogel–solid bonding commonly used in engineering applications as functions of the water concentration in the hydrogels. DOPA in **b** represents 3,4-dihydroxyphenyl-L-alanine. Values in **a** represent the mean and the standard deviation (n = 3–5).

control case, we model the peeling test of a hydrogel with no Mullins effect (that is, no dissipation) but otherwise the same mechanical properties as the tough hydrogel. From Fig. 2j, it is evident that the calculated interfacial toughness for the control case is approximately the same as the prescribed intrinsic work of adhesion. Although the current finite-element model does not account for the effects of fingering instability or viscoelasticity on mechanical dissipation, it clearly demonstrates that high values of the intrinsic work of adhesion and significant mechanical dissipation of the bulk hydrogels are key factors in designing tough bonding of hydrogels on solids (Fig. 2j).

The proposed design strategy and fabrication methods for tough hydrogel–solid bonding is applicable to multiple types of non-porous solid materials. Figure 3a shows that the measured interfacial toughness is consistently high for the PAAm-alginate tough hydrogel chemically anchored on glass (1,500 J m^{-2}), silicon (1,500 J m^{-2}), aluminium (1,200 J m^{-2}), titanium (1,250 J m^{-2}) and ceramics (1,300 J m^{-2}). Replacing the PAAm-alginate with other types of tough hydrogels, including PAAm-hyaluronan, PAAm-chitosan, PEGDA-alginate and PEGDA-hyaluronan, still yields relatively high interfacial toughness values, 148–820 J m^{-2}, compared with the interfacial toughness in controlled cases, 4.4–16 J m^{-2} (Supplementary Fig. 6). (See Methods for details on other hydrogel–solid bonding.) To explain the difference in interfacial toughness of different tough hydrogels with long-chain networks chemically anchored on substrates, we measure the maximum dissipative capacity and fracture toughness of these hydrogels (Supplementary Fig. 7). It can be seen that, for tough hydrogels with the same chemically anchored long-chain networks (that is, PAAm-based or PEGDA-based tough hydrogels), both the interfacial toughness and fracture toughness increase with the maximum dissipative capacity of the hydrogels (Supplementary Fig. 7). These results validate that significant energy dissipation in bulk hydrogels is critical to achieving high interfacial toughness.

As hydrogels are commonly used in wet environments, we further immerse the PAAm-alginate hydrogels with PAAm networks anchored on various solid substrates in water for 24 h to allow the hydrogels to swell to equilibrium states. We find that the anchored hydrogels do not detach from the solid substrates in the swollen state. The interfacial toughness of the swollen samples is measured using the 90-degree-peeling test. From Supplementary Movie 4, it can be seen that the detaching process of the swollen hydrogel is similar to that of the same hydrogel in the as-prepared state (that is, Fig. 2f–h and Supplementary Movie 3). As shown in Supplementary Fig. 8b and Fig. 3a, the measured interfacial toughness values for swollen hydrogels bonded on glass (1,123 J m^{-2}), silicon

($1{,}210\ J\ m^{-2}$), aluminium ($1{,}046\ J\ m^{-2}$), titanium ($1{,}113\ J\ m^{-2}$) and ceramics ($1{,}091\ J\ m^{-2}$) are consistently high, indicating that the design strategy and fabrication methods can give tough bonding of hydrogels to diverse solids in a wet environment. The slight decrease in interfacial toughness from as-prepared to swollen hydrogels may be due to the decrease of dissipative capability of hydrogels[34] and/or the residual stress generated in the hydrogels during swelling.

The above results prove that chemically anchoring the long-chain networks of tough hydrogels on solid substrates can lead to tough hydrogel–solid bonding. As the tough hydrogels used in the current study are composed of covalently crosslinked long-chain networks and reversibly crosslinked dissipative networks, it is also important to know the effects of chemically anchoring dissipative networks on the resultant interfacial toughness. We chemically anchor the dissipative networks (that is, alginate or hyaluronan) in PAAm-alginate, PEGDA-alginate and PEGDA-hyaluronan hydrogels on glass substrates using EDC–Sulfo-NHS chemistry, and then measure the interfacial toughness of resultant samples (see Supplementary Fig. 1b,c and Methods for details on anchoring alginate and hyaluronan). As shown in Supplementary Fig. 9a,b, the measured interfacial toughness for PEGDA-alginate and PEGDA-hyaluronan hydrogels with dissipative networks anchored on substrates is $13\ J\ m^{-2}$ and $16\ J\ m^{-2}$ respectively—much lower than the values of the same hydrogels with long-chain networks anchored on substrates ($365\ J\ m^{-2}$ and $148\ J\ m^{-2}$ respectively). On the other hand, the interfacial toughness for PAAm-alginate hydrogel with alginate anchored on the substrate is $1{,}450\ J\ m^{-2}$ (Supplementary Fig. 9c), similar to the value for PAAm-alginate hydrogel with PAAm anchored on the substrate ($1{,}500\ J\ m^{-2}$). It is evident that anchoring either long-chain or dissipative networks gives similar interfacial toughness in PAAm-alginate hydrogel but very different values in PEGDA-alginate (or PEGDA-hyaluronan) hydrogel (Supplementary Fig. 9). The different results obtained in PAAm-alginate and PEGDA-alginate (or PEGDA-hyaluronan) hydrogels may be due to much stronger interactions between long-chain and dissipative networks in PAAm-alginate hydrogel than in PEGDA-alginate and PEGDA-hyaluronan hydrogels[6,35].

To compare our results with existing works in the field, we summarize the interfacial toughness of various hydrogel–solid bonding commonly used in engineering applications versus water concentration in those hydrogels in Fig. 3b. (See Supplementary Methods and Supplementary Fig. 10 for detailed references.) Whereas our approach allows the PAAm-alginate tough hydrogels to contain 90 wt% of water and does not require porous or topographically patterned surfaces of the solids, it can achieve extremely high interfacial toughness values up to $1{,}500\ J\ m^{-2}$. In comparison, most of synthetic hydrogel bonding has relatively low interfacial toughness, below $100\ J\ m^{-2}$. Although previous work on hydrogels and animal skin tissues impregnated in porous substrates gave interfacial toughness values up to $1{,}000\ J\ m^{-2}$, the hydrogels and tissues contains 60–80 wt% water and the requirement of porous solids significantly limits their applications[18]. Further notably, our fabrication methods for tough hydrogel bonding are relatively simple compared with previous methods, as well as being generally applicable to a wide range of hydrogels and solid materials.

Owing to its simplicity and versatility, the design strategy and fabrication methods for tough hydrogel–solid bonding can potentially enable a set of unprecedented functions of hydrogel–solid hybrids. For example, the tough hydrogels may be used as soft (for example, 30 kPa), wet (for example, with 90% water) and biocompatible[36] superglues for glass, ceramics and Ti, which have been used in biomedical applications. (See Methods and Supplementary Fig. 12 for details on biocompatibility of tough hydrogels bonded on solid surfaces.) Figure 4a demonstrates that two glass plates bonded by the tough hydrogel superglue (dimension, $5\ cm \times 5\ cm \times 1.5\ mm$) are transparent, and can readily sustain a weight of 25 kg. (See Methods for details on fabrication of hydrogel superglue.) As another example, the tough hydrogel–solid bonding can re-define the functions and capabilities of commonly used hydrogel coatings, which are usually mechanically fragile and susceptible to debonding failure. Supplementary Movie 5 and Fig. 4b demonstrate the process of shattering and consequently deforming a silicon wafer coated with a layer of chemically anchored tough hydrogel. Thanks to the high toughness of the hydrogel and interface, the new coating prevents detachment of the shattered pieces of silicon wafer and maintains integrity of the hydrogel–solid hybrid even under a high stretch of three times, demonstrating the hydrogel coating's new capability for mechanical protection and support. (See Methods for details on fabrication of mechanically protective hydrogel coating.) The tough hydrogel bonding can also be used as compliant joints in mechanical and robotic structures. Supplementary Movie 6 and Fig. 4c demonstrate an example of four ceramic bars bonded with the chemically anchored tough hydrogels. The compliance of the hydrogel combined with high toughness of the bonding enables versatile modes of deformation of the structure. (See Methods for details on fabrication of hydrogel joints.) In addition, the tough hydrogel bonding is electrically conductive and thus can provide a robust interface between hydrogel ionic conductors and metal electrodes[16]. Existing hydrogel–metal interfaces usually rely on conductive copper tapes whose robustness is uncertain. Supplementary Movie 7 and Fig. 4d demonstrate that the hybrid combination of a tough hydrogel chemically anchored on two titanium electrodes is conductive enough to power a LED light, even when the hydrogel is under a high stretch of 4.5 times. In addition, the conductivity of the hydrogel–metal hybrid remains almost the same even after 1,000 cycles of high stretch up to four times. (See Methods and Supplementary Fig. 11 for details on the fabrication of robust hydrogel–metal conductors and measurements of the electrical conductivity.)

In summary, we demonstrate that the chemical anchorage of long-chain polymer networks of tough hydrogels on solid surfaces represents a general strategy to design tough and functional bonding between hydrogels and diverse solids. Following the design strategy, we use simple methods such as silane modification and EDC chemistry to achieve tough, transparent and conductive bonding of hydrogels to glass, ceramic, silicon wafer, aluminium and titanium with interfacial toughness values over $1{,}000\ J\ m^{-2}$—superior to the toughness of tendon–bone and cartilage–bone interfaces. High values of the intrinsic work of adhesion and significant mechanical dissipation of the bulk hydrogels are key factors that lead to the tough bonding. The ability to fabricate extremely robust hydrogel–solid hybrids makes a number of future research directions and applications possible. For example, electronic devices robustly embedded in (or attached on) tough hydrogels may lead to a new class of stretchable hydrogel electronics, which are softer, wetter and more biocompatible than existing ones based on dry elastomer matrices. New microfluidic systems based on tough hydrogels bonded on non-porous substrates may be able to sustain high flow rates, high pressure and large deformation to better approximate physiological environments than existing microfluidics based on weak or brittle hydrogels. Neural probes coated with tough and biocompatible hydrogels with reduced rigidity[34] may be used to better match the mechanical and physiological properties of the brain, spinal cord and peripheral nervous systems.

Methods

Methods and any associated references are available in the online version of the paper.

Received 28 May 2015; accepted 25 September 2015; published online 9 November 2015

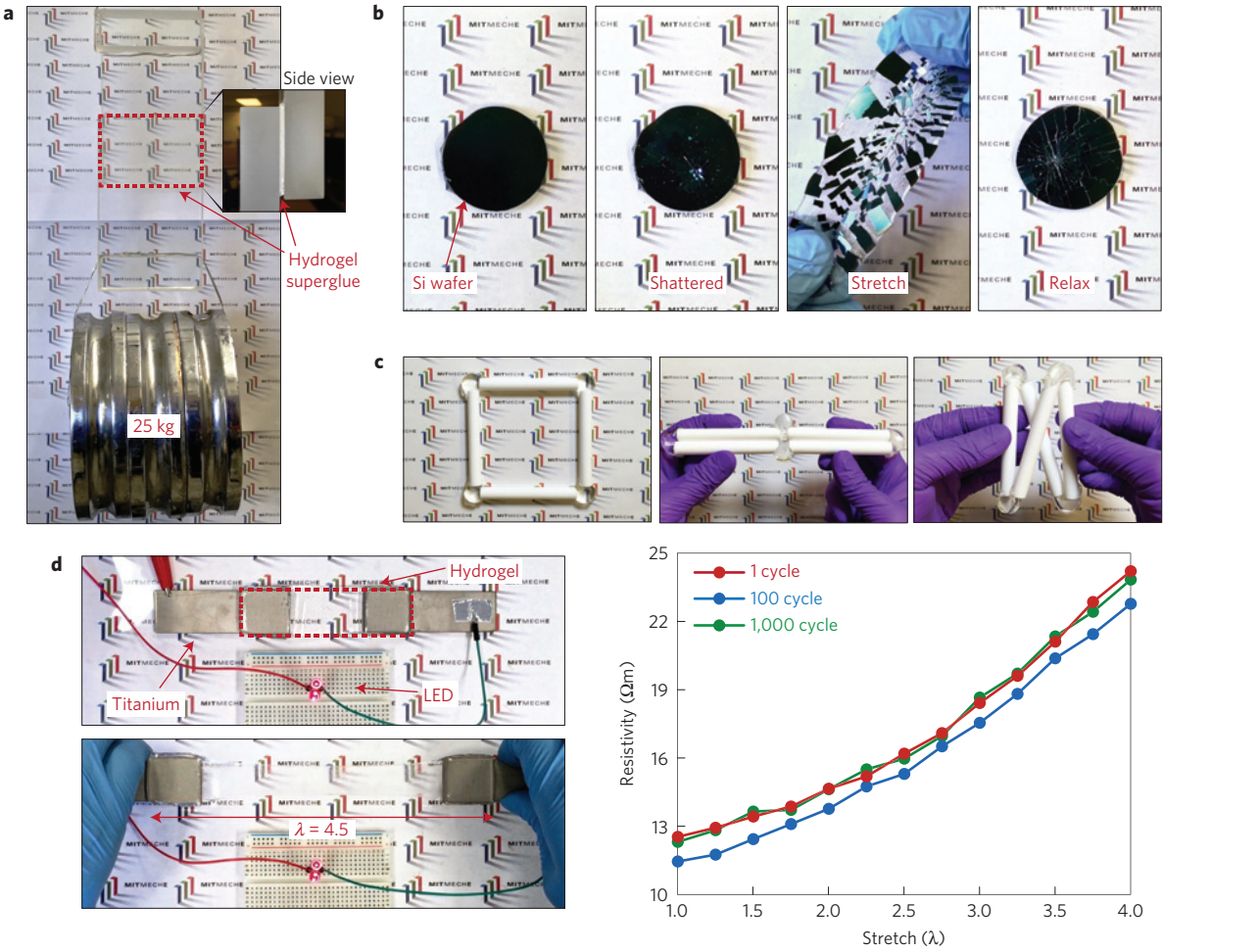

Figure 4 | Novel applications of hydrogel–solid hybrids enabled by the tough bonding. a, Two glass plates bonded by the hydrogel superglue (dimension, 5 cm × 5 cm × 1.5 mm) are transparent, and can readily sustain a weight of 25 kg. **b**, The tough bonding of hydrogel to a silicon wafer gives a new coating that is mechanically protective. Shattered silicon chips still attach tightly to the hydrogel coating even under high stretches. **c**, The tough hydrogel bonding acts as flexible but robust joints between four ceramic bars, which can be deformed into different configurations. **d**, The tough bonding of an ion-containing hydrogel on two titanium electrodes is conductive enough to power a LED light, even when the hydrogel is under a high stretch of 4.5 times. The conductivity of the hydrogel–metal hybrid remains almost the same even after 1,000 cycles of a high stretch up to four times.

References

1. Bobyn, J., Wilson, G., MacGregor, D., Pilliar, R. & Weatherly, G. Effect of pore size on the peel strength of attachment of fibrous tissue to porous-surfaced implants. *J. Biomed. Mater. Res.* **16,** 571–584 (1982).
2. Moretti, M. *et al.* Structural characterization and reliable biomechanical assessment of integrative cartilage repair. *J. Biomech.* **38,** 1846–1854 (2005).
3. Gong, J. P., Katsuyama, Y., Kurokawa, T. & Osada, Y. Double-network hydrogels with extremely high mechanical strength. *Adv. Mater.* **15,** 1155–1158 (2003).
4. Wang, Q. *et al.* High-water-content mouldable hydrogels by mixing clay and a dendritic molecular binder. *Nature* **463,** 339–343 (2010).
5. Henderson, K. J., Zhou, T. C., Otim, K. J. & Shull, K. R. Ionically cross-linked triblock copolymer hydrogels with high strength. *Macromolecules* **43,** 6193–6201 (2010).
6. Sun, J.-Y. *et al.* Highly stretchable and tough hydrogels. *Nature* **489,** 133–136 (2012).
7. Sun, T. L. *et al.* Physical hydrogels composed of polyampholytes demonstrate high toughness and viscoelasticity. *Nature Mater.* **12,** 932–937 (2013).
8. Kamata, H., Akagi, Y., Kayasuga-Kariya, Y., Chung, U.-i. & Sakai, T. "Nonswellable" hydrogel without mechanical hysteresis. *Science* **343,** 873–875 (2014).
9. Liu, M. *et al.* An anisotropic hydrogel with electrostatic repulsion between cofacially aligned nanosheets. *Nature* **517,** 68–72 (2015).
10. Peppas, N. A., Hilt, J. Z., Khademhosseini, A. & Langer, R. Hydrogels in biology and medicine: From molecular principles to bionanotechnology. *Adv. Mater.* **18,** 1345–1360 (2006).
11. Lee, K. Y. & Mooney, D. J. Hydrogels for tissue engineering. *Chem. Rev.* **101,** 1869–1880 (2001).
12. Sidorenko, A., Krupenkin, T., Taylor, A., Fratzl, P. & Aizenberg, J. Reversible switching of hydrogel-actuated nanostructures into complex micropatterns. *Science* **315,** 487–490 (2007).
13. Banerjee, I., Pangule, R. C. & Kane, R. S. Antifouling coatings: Recent developments in the design of surfaces that prevent fouling by proteins, bacteria, and marine organisms. *Adv. Mater.* **23,** 690–718 (2011).
14. Dong, L., Agarwal, A. K., Beebe, D. J. & Jiang, H. Adaptive liquid microlenses activated by stimuli-responsive hydrogels. *Nature* **442,** 551–554 (2006).
15. Beebe, D. J. *et al.* Functional hydrogel structures for autonomous flow control inside microfluidic channels. *Nature* **404,** 588–590 (2000).
16. Keplinger, C. *et al.* Stretchable, transparent, ionic conductors. *Science* **341,** 984–987 (2013).
17. Yu, C. *et al.* Electronically programmable, reversible shape change in two-and three-dimensional hydrogel structures. *Adv. Mater.* **25,** 1541–1546 (2013).
18. Kurokawa, T., Furukawa, H., Wang, W., Tanaka, Y. & Gong, J. P. Formation of a strong hydrogel–porous solid interface via the double-network principle. *Acta Biomater.* **6,** 1353–1359 (2010).
19. Ahagon, A. & Gent, A. Effect of interfacial bonding on the strength of adhesion. *J. Polym. Sci.* **13,** 1285–1300 (1975).
20. Gent, A. Adhesion and strength of viscoelastic solids. Is there a relationship between adhesion and bulk properties? *Langmuir* **12,** 4492–4496 (1996).
21. Kaelble, D. Peel adhesion: Influence of surface energies and adhesive rheology. *J. Adhes.* **1,** 102–123 (1969).

22. Derail, C., Allal, A., Marin, G. & Tordjeman, P. Relationship between viscoelastic and peeling properties of model adhesives. Part 1. Cohesive fracture. *J. Adhes.* **61,** 123–157 (1997).
23. Sudre, G., Olanier, L., Tran, Y., Hourdet, D. & Creton, C. Reversible adhesion between a hydrogel and a polymer brush. *Soft Matter* **8,** 8184–8193 (2012).
24. Weissman, J. M., Sunkara, H. B., Albert, S. T. & Asher, S. A. Thermally switchable periodicities and diffraction from mesoscopically ordered materials. *Science* **274,** 959–963 (1996).
25. Gong, J. P. Why are double network hydrogels so tough? *Soft Matter* **6,** 2583–2590 (2010).
26. Zhao, X. Multi-scale multi-mechanism design of tough hydrogels: Building dissipation into stretchy networks. *Soft Matter* **10,** 672–687 (2014).
27. Lake, G. J. & Thomas, A. G. Strength of highly elastic materials. *Proc. R. Soc. Lond. Ser. A* **300,** 108–119 (1967).
28. Webber, R. E., Creton, C., Brown, H. R. & Gong, J. P. Large strain hysteresis and Mullins effect of tough double-network hydrogels. *Macromolecules* **40,** 2919–2927 (2007).
29. Tegelström, H. & Wyöni, P. I. Silanization of supporting glass plates avoiding fixation of polyacrylamide gels to glass cover plates. *Electrophoresis* **7,** 99 (1986).
30. Kendall, K. Thin-film peeling-the elastic term. *J. Phys. D* **8,** 1449–1452 (1975).
31. Ghatak, A., Chaudhury, M. K., Shenoy, V. & Sharma, A. Meniscus instability in a thin elastic film. *Phys. Rev. Lett.* **85,** 4329–4332 (2000).
32. Biggins, J. S., Saintyves, B., Wei, Z., Bouchaud, E. & Mahadevan, L. Digital instability of a confined elastic meniscus. *Proc. Natl Acad. Sci. USA* **110,** 12545–12548 (2013).
33. Ogden, R. & Roxburgh, D. A pseudo–elastic model for the Mullins effect in filled rubber. *Proc. R. Soc. Lond. Ser. A* **455,** 2861–2877 (1999).
34. Lin, S., Zhou, Y. & Zhao, X. Designing extremely resilient and tough hydrogels via delayed dissipation. *Extreme Mech. Lett.* **1,** 70–75 (2014).
35. Hong, S. *et al.* 3D printing of highly stretchable and tough hydrogels into complex, cellularized structures. *Adv. Mater.* **27,** 4035–4040 (2015).
36. Darnell, M. C. *et al.* Performance and biocompatibility of extremely tough alginate/polyacrylamide hydrogels. *Biomaterials* **34,** 8042–8048 (2013).

Acknowledgements

The authors thank A. Wang and L. Griffith for their help on the cell viability test. This work is supported by ONR (No. N00014-14-1-0528), MIT Institute for Soldier Nanotechnologies and NSF (No. CMMI-1253495). H.Y. acknowledges the financial support from Samsung Scholarship. X.Z. acknowledges the supports from NIH (No. UH3TR000505) and MIT Materials Research Science and Engineering Center.

Author contributions

X.Z. and H.Y. conceived the idea. H.Y., T.Z., S.L., G.A.P. and X.Z. designed the research. H.Y., S.L. and G.A.P. carried out the experiments and T.Z. performed the numerical simulation. H.Y., T.Z., S.L., G.A.P. and X.Z. analysed and interpreted the results. X.Z. drafted the manuscript and all authors contributed to the writing of the manuscript.

Additional information

Supplementary information is available in the online version of the paper. Reprints and permissions information is available online at www.nature.com/reprints. Correspondence and requests for materials should be addressed to X.Z.

Competing financial interests

The authors declare no competing financial interests.

Methods

Materials. Unless otherwise specified, the chemicals used in the current work were purchased from Sigma-Aldrich and used without further purification. For the long-chain polymer networks in the hydrogels, acrylamide (AAm; Sigma-Aldrich A8887) was the monomer used for the polyacrylamide (PAAm) networks, and 20 kDa polyethylene glycol diacrylate (PEGDA) was the macromonomer used for the PEGDA networks. The PEGDA macromonomers were synthesized based on a previously reported protocol[37] using polyethylene glycol (PEG; Sigma-Aldrich 81300), acryloyl chloride (Sigma-Aldrich 549797), triethylamine (TEA; Sigma-Aldrich 471283), dichloromethane (Sigma-Aldrich 270997), sodium bicarbonate (Sigma-Aldrich S6014), magnesium sulphate (Sigma-Aldrich M7506) and diethyl ether (Sigma-Aldrich 346136). For the polyacrylamide (PAAm) hydrogel, *N*,*N*-methylenebisacrylamide (MBAA; Sigma-Aldrich 146072) was used as crosslinker, ammonium persulphate (APS; Sigma-Aldrich A3678) as thermal initiator and *N*,*N*,*N*′,*N*′-tetramethylethylenediamine (TEMED; Sigma-Aldrich T9281) as crosslinking accelerator. For the PEGDA hydrogel, 2-hydroxy-4′-(2-hydroxyethoxy)-2-methylpropiophenone (Irgacure 2959; Sigma-Aldrich 410896) was used as photo initiator. For the dissipative polymer networks in tough hydrogels, a number of ionically crosslinkable biopolymers were used, including sodium alginate (Sigma-Aldrich A2033) ionically crosslinked with calcium sulphate (Sigma-Alginate C3771), chitosan (Sigma-Aldrich 740500) ionically crosslinked with sodium tripolyphosphate (TPP; Sigma-Aldrich 238503), and sodium hyaluronan (HA; Sigma-Aldrich H5542) ionically crosslinked with iron chloride (Sigma-Aldrich 157740). For chemical modification of various solid materials, functional silane 3-(trimethoxysilyl) propyl methacrylate (TMSPMA; Sigma-Aldrich 440159) and acetic acid (Sigma-Aldrich 27225) were used. For anchoring alginate and hyaluronan on solid substrates, (3-aminopropyl) triethoxysilane (APTES, Sigma-Aldrich 440140), *N*-hydroxysulphosuccinimide (Sulfo-NHS, Sigma-Aldrich 56485), *N*-(3-dimethylaminopropyl)-*N*′ ethylcarbodiimide (EDC, Sigma-Aldrich 39391), 2-(*N*-morpholino)ethanesulphonic acid (MES, Sigma-Aldrich M3671) and sodium chloride (Sigma-Aldrich 746398) were used.

In the 90-degree peeling experiments, borosilicate glass (McMaster Carr), silicon wafers with a thermal oxidized layer (UniversityWafer), non-porous glass mica ceramic (McMaster Carr), anodized aluminium (Inventables) and titanium (McMaster Carr) plates were used as the solid substrates. As a stiff backing for the hydrogel sheet, ultrathin glass films (25 μm; Schott Advanced Optics) were used together with transparent Scotch tape (3 M). In the conductive hydrogel–metal bonding experiments, sodium chloride solution was used as an electrolyte.

Synthesis of various tough hydrogels. The PAAm-alginate tough hydrogel was synthesized by mixing 10 ml of a carefully degassed aqueous precursor solution (12.05 wt% AAm, 1.95 wt% sodium alginate, 0.017 wt% MBAA and 0.043 wt% APS) with calcium sulphate slurry (0.1328 times the weight of sodium alginate) and TEMED (0.0025 times the weight of AAm; ref. 6). The mixture was mixed quickly and poured into a laser-cut Plexiglass acrylic mould. The lid of the mould included an opening for the functionalized substrates to be in contact with hydrogel precursor solution. The gel was crosslinked by ultraviolet light irradiation for an hour (254 nm exposure with 6.0 mW cm^{-2} average intensity; Spectrolinker XL-1500).

The PAAm-hyaluronan tough hydrogel was synthesized by mixing 10 ml of degassed precursor solution (18 wt% AAm, 2 wt% HA, 0.026 wt% MBAA and 0.06 wt% APS) with 60 μl of iron chloride solution (0.05 M) and TEMED (0.0025 times the weight of AAm). The PAAm-chitosan tough hydrogel was synthesized by mixing 10 ml of degassed precursor solution (24 wt% AAm, 2 wt% chitosan, 0.034 wt% MBAA and 0.084 wt% APS) with 60 μl of TPP solution (0.05 M) and TEMED (0.0025 times the weight of AAm). The PEGDA-alginate tough hydrogel was synthesized by mixing 10 ml of a degassed precursor solution (20 wt% PEGDA and 2.5 wt% sodium alginate) with calcium sulphate slurry (0.068 times the weight of sodium alginate) and Irgacure 2959 (0.0018 the weight of PEGDA). The PEGDA-hyaluronan tough hydrogel was synthesized by mixing 10 ml of a degassed precursor solution (20 wt% PEGDA and 2 wt% HA) with 60 μl of iron chloride solution (0.05 M) and Irgacure 2959 (0.0018 the weight of PEGDA). The curing procedure was identical to that used for the PAAm-alginate tough hydrogel.

Common PAAm hydrogel was synthesized by mixing 10 ml of degassed precursor solution (23 wt% AAm, 0.051 wt% MBAA and 0.043 wt% APS) and TEMED (0.0025 times the weight of AAm). The curing procedure was identical to that used for the PAAm-alginate tough hydrogel. Note that the modulus of the common PAAm hydrogel was tuned to match the PAAm-alginate tough hydrogel's modulus (30 kPa) based on the previously reported data[6].

Chemically anchoring PAAm and PEGDA on various solid surfaces. The surface of various solids was functionalized by grafting functional silane TMSPMA. Solid substrates were thoroughly cleaned with acetone, ethanol and deionized water in that order, and completely dried before the next step. Cleaned substrates were treated by oxygen plasma (30 W at a pressure of 200 mtorr; Harrick Plasma PDC-001) for 5 min. Immediately after the plasma treatment, the substrate surface was covered with 5 ml of the silane solution (100 ml deionized water, 10 μl of acetic acid with pH 3.5 and 2 wt% of TMSPMA) and incubated for 2 h at room temperature. Substrates were washed with ethanol and completely dried. Functionalized substrates were stored in low-humidity conditions before being used for experiments.

During oxygen plasma treatment of the solids, oxide layers on the surfaces of the solids (silicon oxide on glass and silicon wafer, aluminium oxide on aluminium, titanium oxide on titanium, and metal oxides on ceramics) react to hydrophilic hydroxyl groups by oxygen radicals produced by the oxygen plasma. These hydroxyl groups on the oxide layer readily form hydrogen bonds with silanes in the functionalization solution, generating a self-assembled layer of silanes on the oxide layers[38]. Notably, the methoxy groups in TMSPMA are readily hydroxylated in an acidic aqueous environment and formed silanes. These hydrogen bonds between surface oxides and silanes become chemically stable siloxane bonds on the removal of water, forming strongly grafted TMSPMA onto oxide layers on various solids[39].

Grafted TMSPMA has a methacrylate terminal group which can copolymerize with the acrylate groups in either AAm or PEGDA under a free radical polymerization process, generating chemically anchored long-chain polymer networks onto various solid surfaces[40]. Because the long-chain polymer networks in hydrogels are chemically anchored onto solid surfaces via strong and stable covalent bonds, the interfaces can achieve a higher intrinsic work of adhesion than physically attached hydrogels. The silane functionalization chemistry is summarized in Supplementary Fig. 1a.

Chemically anchoring alginate and hyaluronan on various solid surfaces. We anchored alginate and hyaluronan via EDC–Sulfo-NHS chemistry following previously reported protocols[41,42] (Supplementary Fig. 1b,c). Glass substrates were cleaned and treated with oxygen plasma following the above-mentioned procedures and covered with 5 ml of the amino-silane solution (100 ml deionized water, 2 wt% of APTES), then incubated for 2 h at room temperature. Substrates were washed with ethanol and completely dried. The amino-silane functionalized glass substrates were further incubated in either alginate anchoring solution or hyaluronan anchoring solution (100 ml of aqueous MES buffer (0.1 M MES and 50 mM sodium chloride), 1 wt% alginate or hyaluronan, Sulfo-NHS (molar ratio of 30:1 to either alginate or hyaluronan) and EDC (molar ratio of 25:1 to either alginate or hyaluronan)) for 24 h. Incubated glass substrates were finally washed with deionized water and completely dried before use.

Interfacial toughness measurement. All tests were conducted in ambient air at room temperature. The hydrogels and hydrogel–solid interfaces maintain consistent properties over the time of the tests (that is, ∼ a few minutes), during which the effect of dehydration is not significant. Whereas long-term dehydration will significantly affect the properties of hydrogels, adding highly hydratable salts into the hydrogels can enhance their water retention capacity[43]. The interfacial toughness of various hydrogel–solid bondings was measured using the standard 90-degree peeling test (ASTM D 2861) with a mechanical testing machine (2 kN load cell; Zwick/Roell Z2.5) and a 90-degree peeling fixture (TestResources, G50). All rigid substrates were prepared with dimensions 7.62 cm in width, 12.7 cm in length and 0.32 cm in thickness. Hydrogels were cured on the solid substrates in a Plexiglass acrylic mould with a size of 110 mm × 30 mm × 6 mm. As a stiff backing for the hydrogel, TMSPMA-grafted ultrathin glass film was used with an additional protective layer of transparent Scotch tape (3 M) on top of the glass film. Prepared samples were tested with the standard 90-degree peeling test set-up (Supplementary Fig. 2). All 90-degree peeling tests were performed with a constant peeling speed of 50 mm min^{-1}. The measured force reached a plateau as the peeling process entered the steady state, and this plateau force was calculated by averaging the measured force values in the steady-state region with common data processing software (Supplementary Fig. 8a). The interfacial toughness Γ was determined by dividing the plateau force F by the width of the hydrogel sheet W. To test the dependence of interfacial toughness on hydrogel thickness, we carried out a set of 90-degree peeling tests on PAAm-alginate hydrogels with different thicknesses (1.5 ∼ 6 mm) chemically anchored on glass substrates (Supplementary Fig. 4a). For interfacial toughness measurements of fully swollen samples, each peeling test sample was immersed in deionized water for 24 h and tested by the standard 90-degree peeling test (Supplementary Fig. 8b).

To demonstrate the peeling rate dependency of the measured interfacial toughness, we performed a set of 90-degree peeling tests on PAAm-alginate hydrogels chemically anchored on glass substrates with various peeling rates from 5 mm min^{-1} (lowest) to 200 mm min^{-1} (highest; Supplementary Fig. 5).

To demonstrate that the proposed strategy and method is generally applicable to multiple types of hydrogels, we also performed standard 90-degree peeling tests on various types of tough hydrogels, including PAAm-hyaluronan, PAAm-chitosan, PEGDA-alginate and PEGDA-hyaluronan hydrogels chemically anchored on glass substrates (Supplementary Fig. 6a). The measured interfacial toughness for these tough hydrogels (148–820 J m^{-2}, Supplementary Fig. 6b) was consistently much higher than the interfacial toughness of the control cases (4.4–16 J m^{-2}, Supplementary Fig. 6b).

Preparation of hydrogel superglue, coating and joints. For the hydrogel superglue, two TMSPMA-grafted glass plates (5 cm × 12 cm × 2 cm) were connected by thin tough hydrogel (5 cm × 5 cm × 1.5 mm) and subjected to weights up to 25 kg. Weight was applied by hanging metal pieces of known weight with metal wires. Hydrogel joints were fabricated by curing tough hydrogel using a Plexiglass acrylic mould between four TMSPMA-grafted non-porous glass mica ceramic rods (75 mm length with 10 mm diameter), forming an interconnected square structure. To test the robustness of these hydrogel joints, each joint was twisted and rotated to large angles. The hydrogel coating was fabricated by curing a thin (1 mm) tough hydrogel layer onto the TMSPMA-grafted thermal oxide silicon wafer (100 μm thickness with 50.8 mm diameter). To test the hydrogel coating's protective capability, we shattered the wafer with a metal hammer and stretched the hydrogel-coated wafer by hand up to three times its original diameter. In the preparation of samples, we used the PAAm-alginate tough hydrogel. The grafting of TMSPMA on various solids was conducted as discussed in the previous section.

Electrically conductive hydrogel interface. Ionic tough hydrogel was prepared by curing tough PAAm-alginate hydrogel on two TMSPMA-grafted titanium slabs and then soaking in sodium chloride solution (3 M) for 6 h. The electric resistance of the ionic hydrogel–titanium hybrid was measured using the four-point method[44]. The ionic hydrogel–titanium hybrid was connected in series with a function generator and galvanometer, and the voltage between the titanium slabs was measured with a voltmeter connected in parallel (Supplementary Fig. 11a). The ratio of the measured voltage to the measured current gave the electrical resistance of the ionic hydrogel–titanium hybrid. The resistivity was then calculated using the relation $R = \rho L/A$ for a given geometry of the ionic hydrogel in the test where ρ is the resistivity, L is the length of the gel and A is the cross-sectional area. The rate of stretch was kept constant at 100 mm min^{-1} using a mechanical testing machine. All electrical connections other than the ionic tough hydrogel–titanium interface were established using conductive aluminium tape. Cyclic extension of the ionic tough hydrogel was done by a mechanical testing machine based on a predetermined number of cycles. The ionic tough hydrogel's ability to transmit power was tested by lighting up LEDs using an a.c. power source (1 kHz 5 V peak-to-peak sinusoidal). Supplementary Fig. 11b illustrates the test set-up.

Biocompatibility of tough hydrogel bonding. The biocompatibility of tough hydrogels, including PAAm-alginate and PEGDA-alginate hydrogels, has been validated in previous studies[35,36]. In the current study, the biocompatibility of PAAm-alginate hydrogel bonded on silane-grafted glass was tested *in vitro* with a live/dead viability assay of hTERT-immortalized human mesenchymal stem cells (MSCs; Supplementary Fig. 12). A hydrogel disk was chemically anchored on a glass slide following the above-mentioned procedure using TMSPMA and then swelled in PBS for two days. To focus on the biocompatibility of the hydrogel–solid interface, the hydrogel was peeled off from the glass slide to expose the previously bonded interface. Thereafter, both the hydrogel and the glass slide were placed in 24-well plates with the exposed interfaces facing up (Supplementary Fig. 12a). MSCs were seeded at a density of 25,000 cells/well on the exposed interfaces of the hydrogel and glass, and incubated for seven days at 37 °C and 5% CO_2 in complete cell culture media (high-glucose DMEM with 10% FBS, 1 mM sodium pyruvate, 1× MEM (non-essential amino acids), 2 mM glutamax, and 100 U ml^{-1} penicillin–streptomycin) from Life Technologies.

A live/dead staining was performed using the LIVE/DEAD kit for mammalian cells (Life Technologies) according to the manufacturer's instructions, and fluorescent images were obtained using a Leica DMI 6000 microscope with Oasis Surveyor software. As seen in Supplementary Fig. 12c, the MSCs proliferated and survived on the exposed interface of the glass slide. On the exposed interface of the hydrogel, there were fewer cells as the MSCs did not attach well to the hydrogel, but most cells that attached were alive, consistent with previous report[36] (Supplementary Fig. 12b). In both cases, the percentage of viable MSCs on the exposed interfaces is over 95% after seven days of incubation. (It should be noted that although the formed tough hydrogel–glass interface is biocompatible, the bonding process is not, as the AAm monomers used in the process are toxic.)

References

37. Nemir, S., Hayenga, H. N. & West, J. L. PEGDA hydrogels with patterned elasticity: Novel tools for the study of cell response to substrate rigidity. *Biotechnol. Bioeng.* **105,** 636–644 (2010).
38. Dugas, V. & Chevalier, Y. Surface hydroxylation and silane grafting on fumed and thermal silica. *J. Colloid Interface Sci.* **264,** 354–361 (2003).
39. Yoshida, W., Castro, R. P., Jou, J.-D. & Cohen, Y. Multilayer alkoxysilane silylation of oxide surfaces. *Langmuir* **17,** 5882–5888 (2001).
40. Muir, B. V., Myung, D., Knoll, W. & Frank, C. W. Grafting of cross-linked hydrogel networks to titanium surfaces. *ACS Appl. Mater. Interfaces* **6,** 958–966 (2014).
41. Cha, C. *et al.* Tailoring hydrogel adhesion to polydimethylsiloxane substrates using polysaccharide glue. *Angew. Chem. Int. Ed.* **52,** 6949–6952 (2013).
42. Stile, R. A., Barber, T. A., Castner, D. G. & Healy, K. E. Sequential robust design methodology and X-ray photoelectron spectroscopy to analyze the grafting of hyaluronic acid to glass substrates. *J. Biomed. Mater. Res.* **61,** 391–398 (2002).
43. Bai, Y. *et al.* Transparent hydrogel with enhanced water retention capacity by introducing highly hydratable salt. *Appl. Phys. Lett.* **105,** 151903 (2014).
44. Yang, C. H. *et al.* Ionic cable. *Extreme Mech. Lett.* **3,** 59–65 (2015).

nature materials

SUPPLEMENTARY INFORMATION

DOI: 10.1038/NMAT4463

Tough bonding of hydrogels to diverse non-porous surfaces

*Hyunwoo Yuk[1], Teng Zhang[1], Shaoting Lin[1], German Alberto Parada[1,2], Xuanhe Zhao[1,3]**

[1.] *Soft Active Materials Laboratory, Department of Mechanical Engineering, Massachusetts Institute of Technology, Cambridge, MA 02139, USA;* [2.] *Department of Chemical Engineering, Massachusetts Institute of Technology, Cambridge, MA 02139;* [3.] *Department of Civil and Environmental Engineering, Massachusetts Institute of Technology, Cambridge, MA 02139, USA*

* To whom correspondence should be addressed. Email: zhaox@mit.edu

NUMERICAL MODEL FOR 90-DEGREE PEELING OF TOUGH HYDROGEL

We developed a two-dimensional (2D) finite-element model to simulate the 90-degree-peeling test of hydrogels bonded on solid substrates. As shown in **Fig. S13**, a hydrogel strip with length 80 mm and thickness 0.8~6 mm was adhered on a solid substrate, where a portion of the gel strip (30 mm) was initially detached. The deformation of the hydrogel strip was assumed to be under plane-strain condition. The elastic properties and energy dissipation of the hydrogel were modeled as the Ogden hyperelastic material and Mullins effect[1], respectively. The parameters of the model were obtained by fitting the model to experimental data from mechanical tests on the PAAm-alginate hydrogel[2] (**Fig. S14a**). For the elastic properties, the one-term Ogden model can be expressed as

$$U_{ela} = 2\mu/\alpha^2(\lambda_1^\alpha + \lambda_2^\alpha + \lambda_3^\alpha - 3)$$

DOI: 10.1038/NMAT4463

where U_{ela} is the strain energy density, λ_i the i_{th} principal stretch, μ the shear modulus (fitted to be 36.57 kPa), and α the Ogden parameter (fitted to be 1.473). The theoretical model for the Mullins effect can be expressed as

$$U = \eta \widetilde{U}_{ela} + \phi(\eta)$$

$$\phi(\eta) = \int_1^{\eta} [(m + \beta U_{ela}^m)\text{erf}^{-1}\big(r(1-\eta)\big) - U_{ela}^m] d\eta$$

$$\eta = 1 - \frac{1}{r}\text{erf}[(U_{ela}^m - \widetilde{U}_{ela})/(m + \beta U_{ela}^m)]$$

where η is a damage variable ($0 < \eta \leq 1$), $\widetilde{U}_{ela}$ is the strain energy density of perfectly elastic material (i.e., the primary loading path is also the unloading path), U_{ela}^m denotes the maximum strain energy density before unloading, the function $\phi(\eta)$ is referred to as the damage function, erf is the error function, and the material parameters r = 1.1, m = 4.076, and β = 0.2818 were obtained by fitting the model to measured stress-strain hysteresis of the PAAm-alginate hydrogel[2].

The stiff backing was modeled as a linear elastic material with very high Young's modulus (i.e., 2 GPa) and very low thickness (i.e., 100 μm). The cohesive layer on the interface was characterized by a triangular cohesive law with maximum strength $S_{\max}$ and maximum separation distance $\delta_{\max}$ (**Fig. S14b**). The damage of the cohesive layer follows the quadratic nominal stress criterion,

$$\left\{\frac{t_n}{S_{max}}\right\}^2 + \left\{\frac{t_s}{S_{max}}\right\}^2 = 1$$

where $t_i(n, s)$ represents the nominal stress, and the subscript n and s indicate deformation normal to and tangential to the interface , respectively.

All the numerical simulations were carried out with ABAQUS/Explicit. The hydrogel and stiff backing were modeled with CPE4R element, and the cohesive layer at the interface was modeled with COH2D element. The Poisson's ratio of the hydrogel was set to be 0.499 to approximate incompressibility. The adhesive interface was uniformly discretized with very fine mesh size (0.1 mm).

We also performed simulations with an even finer mesh size (0.05 mm), which gave similar peeling forces and thus verified the mesh insensitivity of our model (**Fig. S15**). Mass scaling technique was adopted to maintain a quasi-static process during the peeling simulations. To simulate the peeling test described in the material and experiment section, the left edge of the strip was first rotated 90 degrees and then moved vertically at a constant velocity, with the reaction force on the left edge of the strip recorded. The interfacial toughness was then calculated as the steady-state reaction force divided by the width of the strip, which is set to be unity in the current model.

To validate the numerical model, we first simulated the peeling process of a pure elastic material without energy dissipation. To prescribe different intrinsic work of adhesion Γ_0 in the cohesive zone, we fixed S_{max} to be 500 kPa and varied δ_{max} from 0.2 to 1.2 mm. **Figure S16a** gives the calculated curves of peeling force per unit width of hydrogel vs. vertical displacement for different values of Γ_0. As demonstrated in **Fig. S16b**, the calculated interfacial toughness for a pure elastic material Γ was indeed very close to the intrinsic work of adhesion Γ_0, indicating that our numerical model is capable of accurately calculating the interfacial toughness. We then simulated the same peeling tests for PAAm-alginate hydrogels with energy dissipation and presented the results in **Fig. S17**. It can be found that the energy dissipation can lead to an interfacial toughness four times of the baseline intrinsic work of adhesion. The simulation snapshots of the peeling process in **Fig. S18** also confirm that a process zone with significant energy dissipation formed during the interfacial crack propagation. For the materials without energy dissipation, the interfacial crack reached the steady state immediately after its initiation (**Fig. S18d-e**) while there was a crack growth stage from the crack initiation to the final steady state for the materials with energy dissipation (**Fig. S18a-c**). We also tested the effect of hydrogel thickness on the interfacial toughness with the finite-element model. As shown in **Fig. S19**, the calculated interfacial toughness was very close to each other for the thickness in the range of 1.5 mm – 6 mm, which was consistent with our experimental measurements.

DOI: 10.1038/NMAT4463

SUPPLEMENTARY FIGURES AND FIGURE CAPTIONS

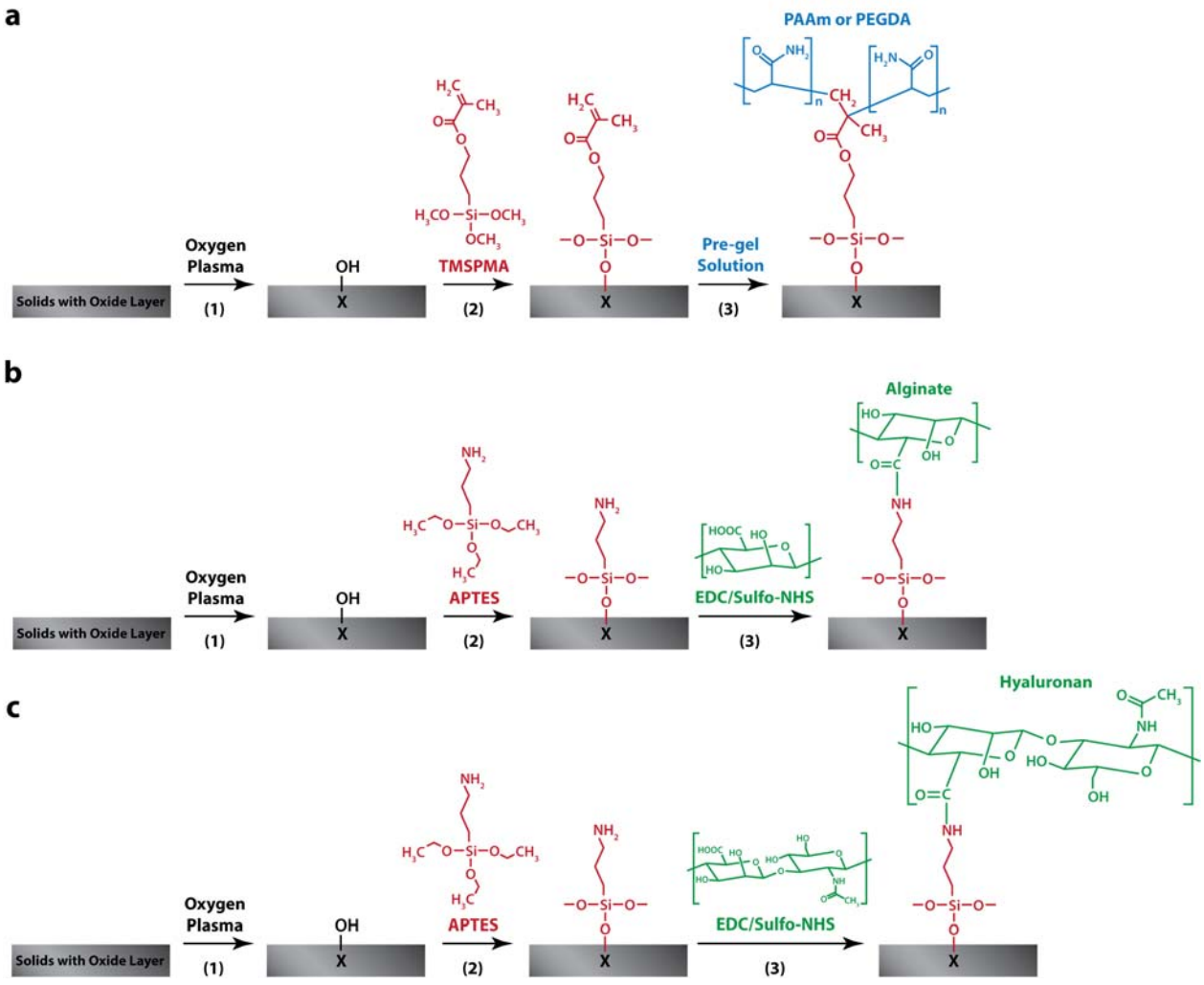

Figure S1. Schematic illustration of the methods to chemically anchor long-chain polymer networks or dissipative polymer networks on various solid surfaces. a. The solid substrates including glass, ceramic, aluminum and titanium were exposed to oxygen plasma to introduce hydroxyl-activated surface oxides on their surfaces. Functional silane TMSPMA was then grafted onto the hydroxyl-activated surface through siloxane covalent chemistry. **b.** Alginate is grafted using EDC-Sulfo NHS chemistry on amino-silane functionalized substrates. **c.** Hyaluronan is grafted using the same EDC-Sulfo NHS chemistry on amino-silane functionalized substrates.

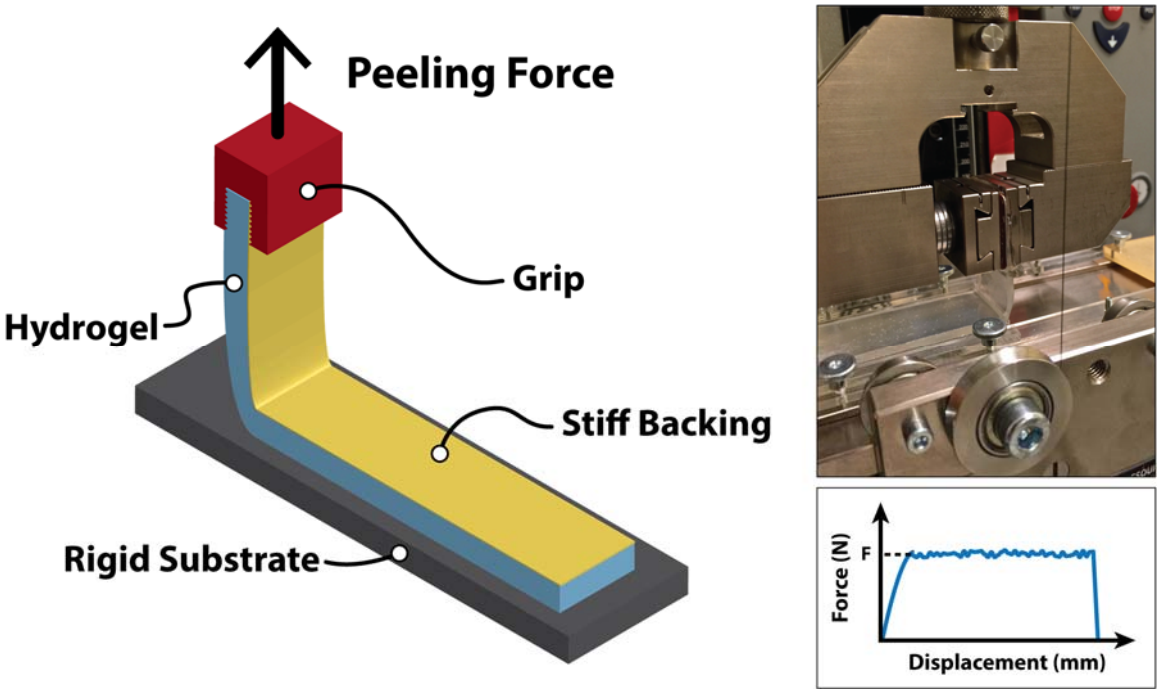

Figure S2. Schematics and experimental setup for the 90-dgree peeling test. Mechanical testing machine (Zwick / Roell Z2.5) pulled the hydrogel sheet together with stiff backing in 90 degrees from the substrate. The peeling fixture (TestResources, G50) maintained the peeling angle to be 90 degrees during the test via a pulley connected to the crosshead of the machine (test standard: ASTM D 2861). The peeling test samples were prepared with 110 mm in length, 30 mm in width and 1.5 – 6 mm in thickness. A glass film with thickness of 25 μm was used as a stiff backing for the hydrogel. The interfacial toughness was calculated by dividing the steady-state (or plateau) peeing force with the sample width.

DOI: 10.1038/NMAT4463

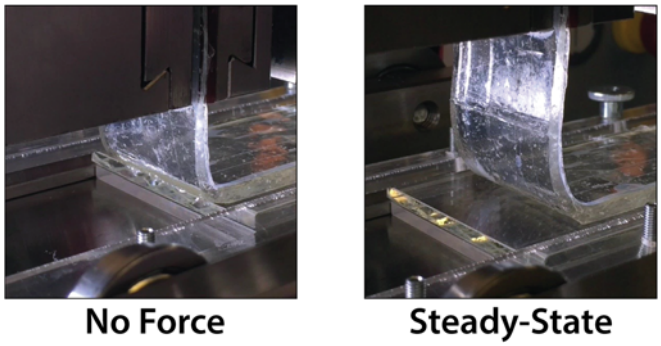

Figure S3. Photos of the peeling process of tough or common hydrogel physically attached on a glass substrate. The crack can easily propagate along the interface without kinking or significantly deforming the hydrogel, giving very low interfacial toughness of 8 Jm^{-2}.

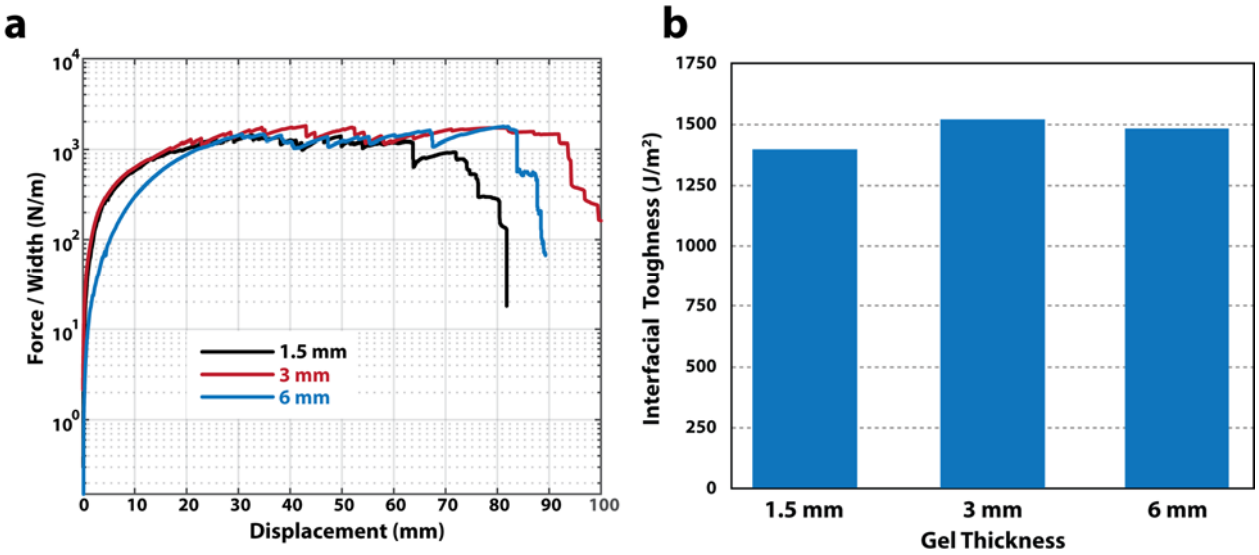

Figure S4. Interfacial toughness of as prepared PAAm-alginate hydrogels with different thicknesses chemically anchored on glass substrates. a. Typical curves of the peeling force per hydrogel width vs. displacement for samples with thickness of 1.5 mm, 3 mm and 6 mm, respectively. **b.** The measured interfacial toughness of as prepared samples with thickness of 1.5 mm, 3 mm and 6 mm, respectively. The interfacial toughness does not significantly depend on sample thickness in this range of 1.5 mm – 6 mm.

DOI: 10.1038/NMAT4463

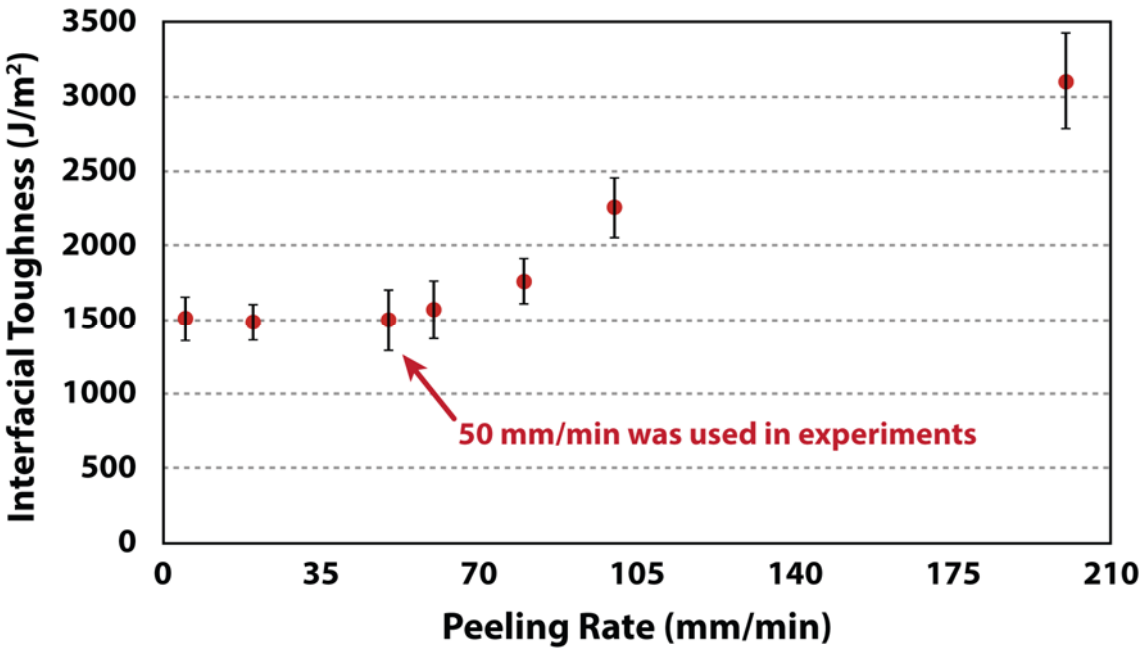

Figure S5. Peeling-rate dependence of measured interfacial toughness of PAAm-algiante hydrogels chemically anchored on glass. The measured interfacial toughness decreases from 3100 Jm^{-2} to 1500 Jm^{-2} as the peeling rate decreases from 200 mm/min to 5 mm/min. Note that the peeling rate used in the current study (50 mm/min) gives an interfacial toughness around the lower asymptote (1500 Jm^{-2}). Values represent mean and standard deviation (n = 3-5).

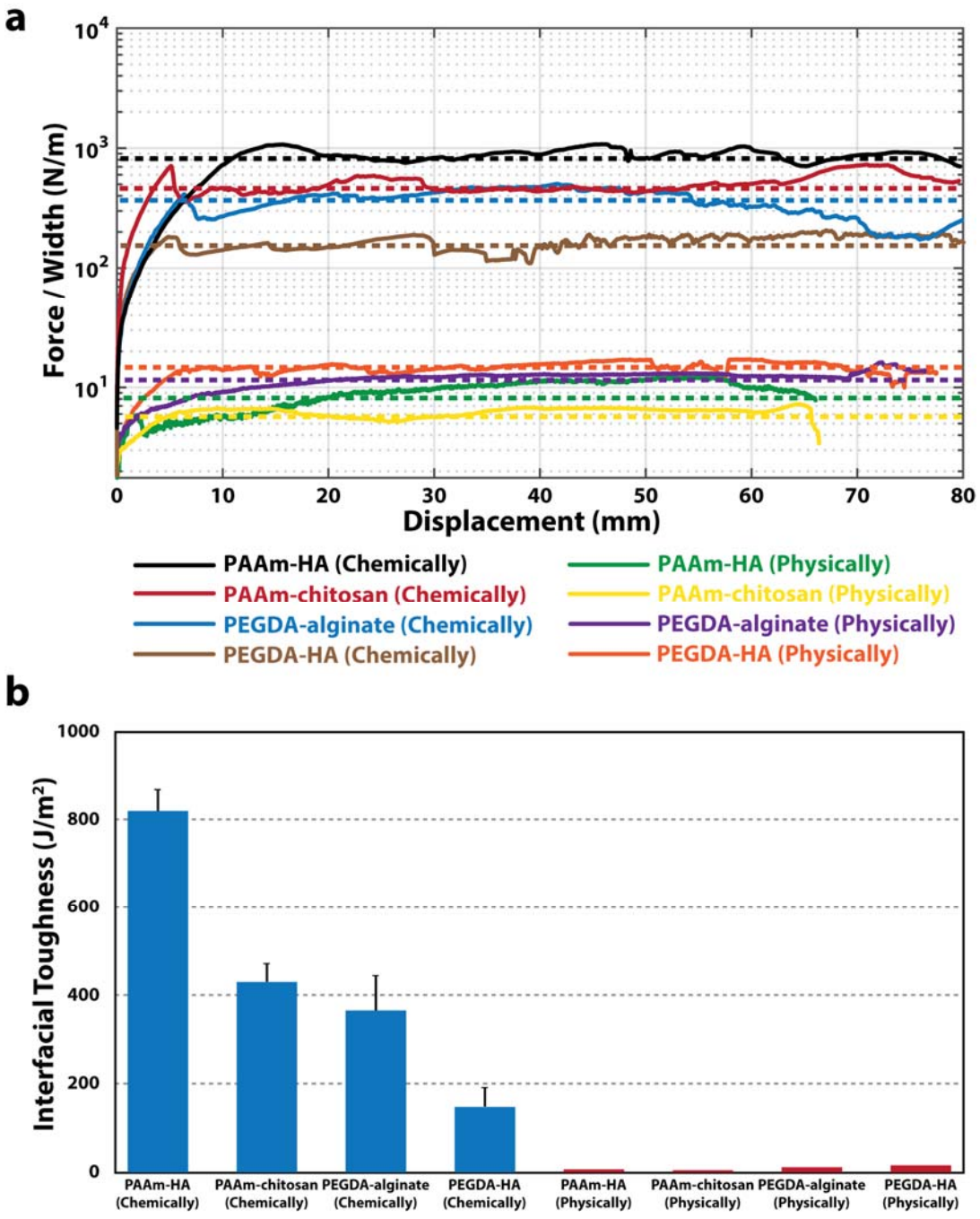

Figure S6. Interfacial toughness for various as-prepared tough hydrogels chemically anchored or physically attached on glass substrates. a. Typical curves of peeling force per hydrogel width vs. displacement for various tough hydrogels chemically anchored or physically attached on glass substrates. **b.** The measured interfacial toughness for various as-prepared tough hydrogels chemically anchored or physically attached on glass substrates. Values in **b.** represent mean and standard deviation (n = 3-5).

DOI: 10.1038/NMAT4463

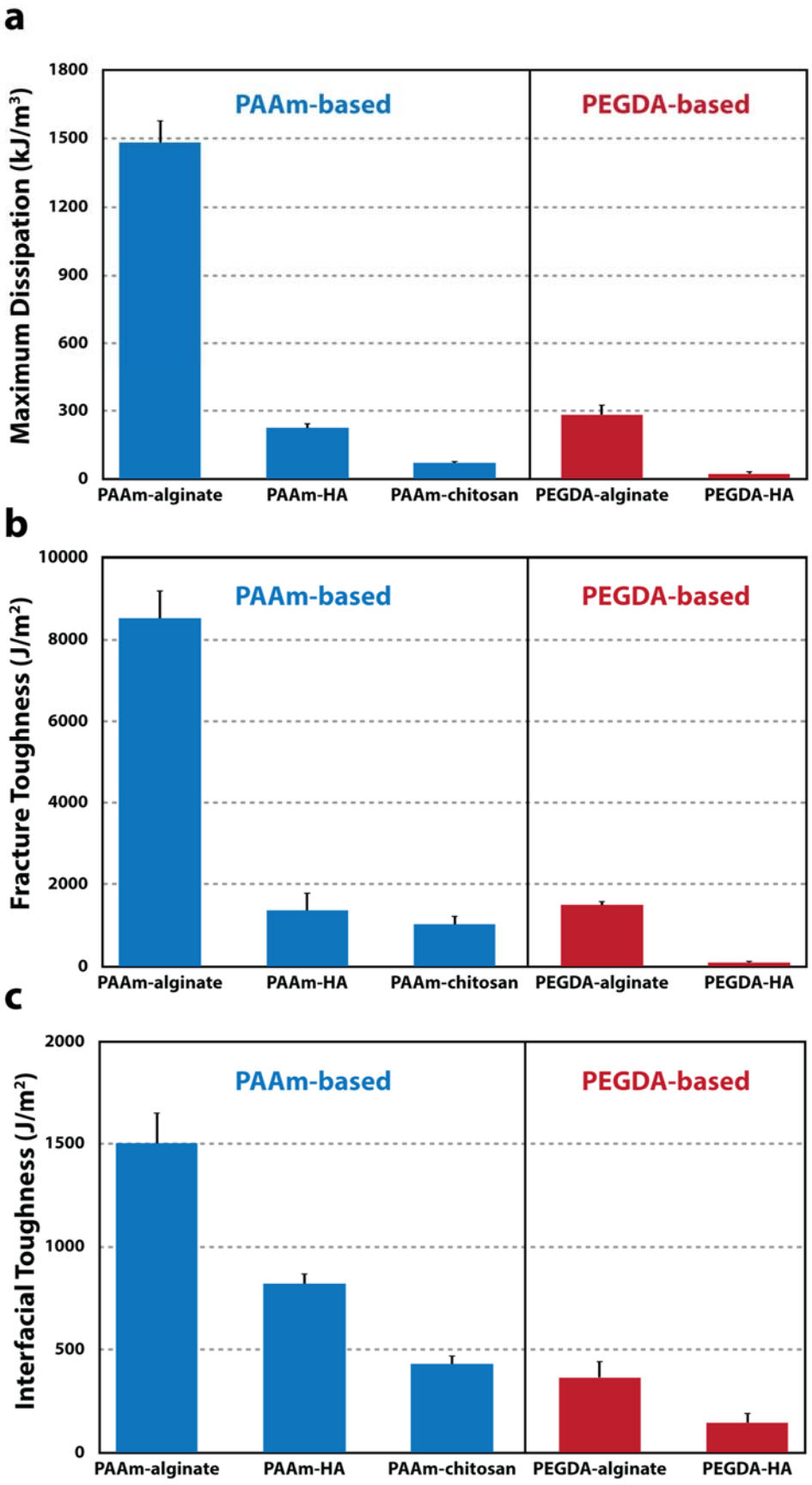

Figure S7. Maximum dissipative capacity, fracture toughness and interfacial toughness of various tough hydrogels with long-chain networks chemically anchored on substrates. a. Maximum dissipative capacity (i.e., area of the maximum stress-stretch hysteresis loop of a sample under pure-shear tensile test) of various PAAm-based and PEGDA-based hydrogels. **b.** Fracture toughness of various PAAm-based and PEGDA-based hydrogels. **c.** Interfacial toughness of various PAAm-based and PEGDA-based hydrogels with long-chain networks chemically anchored on silane-functionalized glass substrates. Values in **a-c.** represent mean and standard deviation (n = 3-5).

DOI: 10.1038/NMAT4463

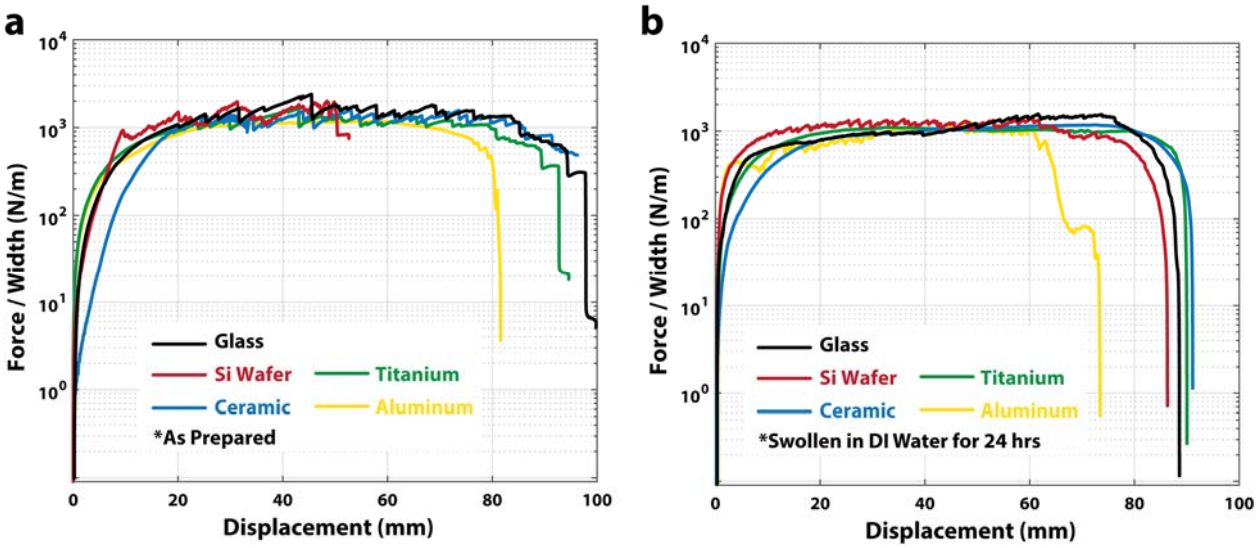

Figure S8. Typical curves of peeling force per hydrogel width vs. displacement for PAAm-alginate hydrogels chemically anchored on various solids. a. The measured interfacial toughness is consistently high for the as prepared PAAm-alginate hydrogel chemically anchored on glass (1500 Jm^{-2}), silicon (1500 Jm^{-2}), aluminum (1200 Jm^{-2}), titanium (1250 Jm^{-2}) and ceramics (1300 Jm^{-2}). **b.** The measured interfacial toughness is still high for the fully swollen PAAm-alginate hydrogel chemically anchored on glass (1123 Jm^{-2}), silicon (1210 Jm^{-2}), aluminum (1046 Jm^{-2}), titanium (1113 Jm^{-2}) and ceramics (1091 Jm^{-2}).

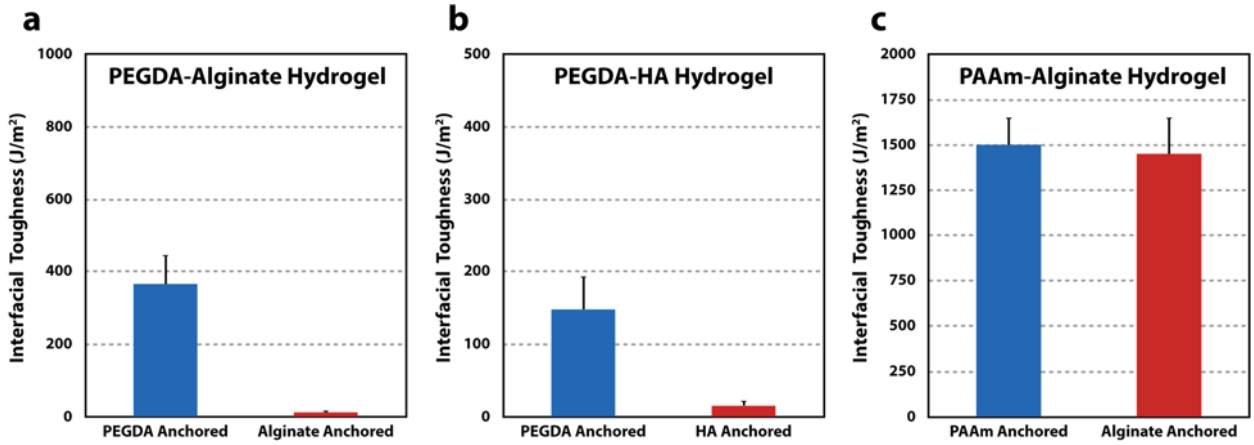

Figure S9. The effect of anchoring dissipative polymer network on interfacial toughness. a. The measured interfacial toughness for PEGDA-alginate with alginate anchored on substrates is 13 Jm^{-2}, much lower than the values of PEGDA-alginate with PEGDA anchored on substrates (365 Jm^{-2}). **b.** The measured interfacial toughness for PEGDA-hyaluronan with hyaluronan anchored on substrates is 16 Jm^{-2}, much lower than the values of PEGDA- hyaluronan with PEGDA anchored on substrates (148 Jm^{-2}). **c.** The interfacial toughness for PAAm-alginate with alginate anchored substrates is 1450 Jm^{-2}, similar to the value of PAAm-alginate with PAAm anchored on substrates (1500 Jm^{-2}). Values in **a-c**. represent mean and standard deviation (n = 3-5).

DOI: 10.1038/NMAT4463

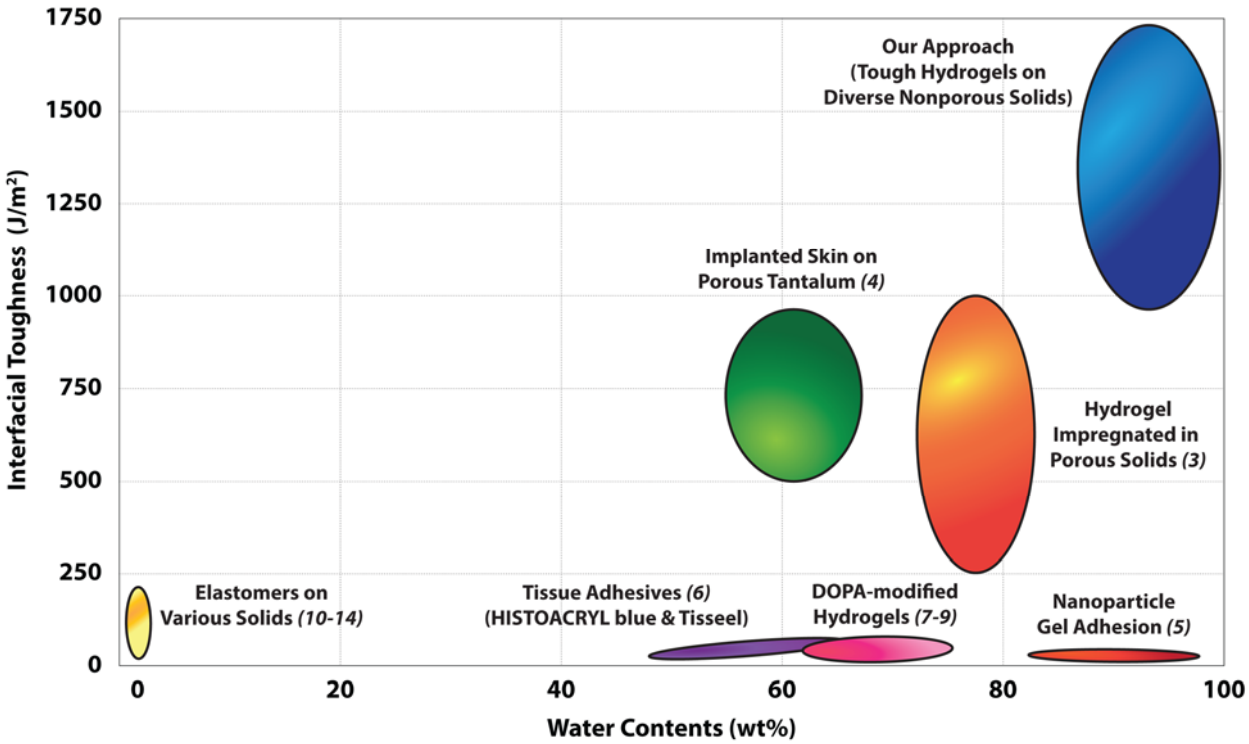

Figure S10. Comparison of interfacial fracture toughness of various hydrogel-solid bonding commonly used in engineering applications as functions of water concentrations in the hydrogels, and the references for the values[3-14].

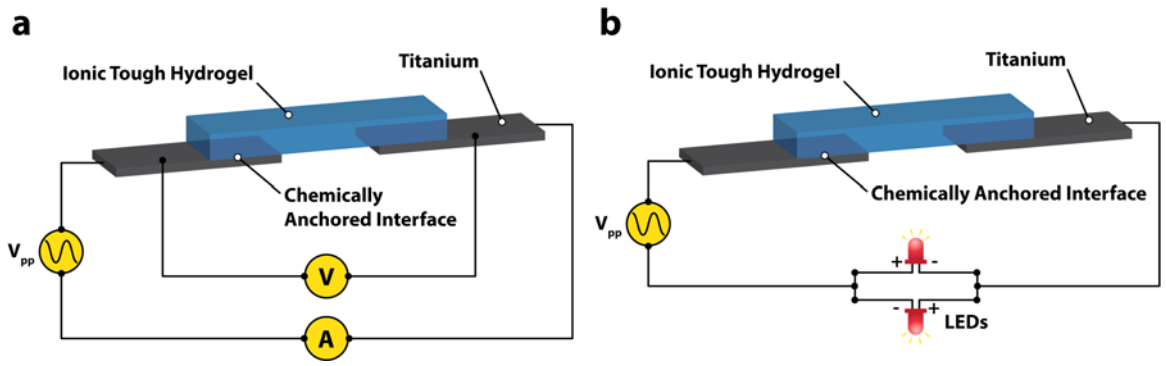

Figure S11. Schematic illustrations for experiments on conductive hydrogel-metal interface. a. Experimental setup for resistivity measurement of ionic tough hydrogel bonded on titanium slabs. **b.** Experimental setup for illustration of power transmission by lighting up LEDs with transmitted power from AC power source through ionic tough hydrogel bonded on titanium slabs.

DOI: 10.1038/NMAT4463

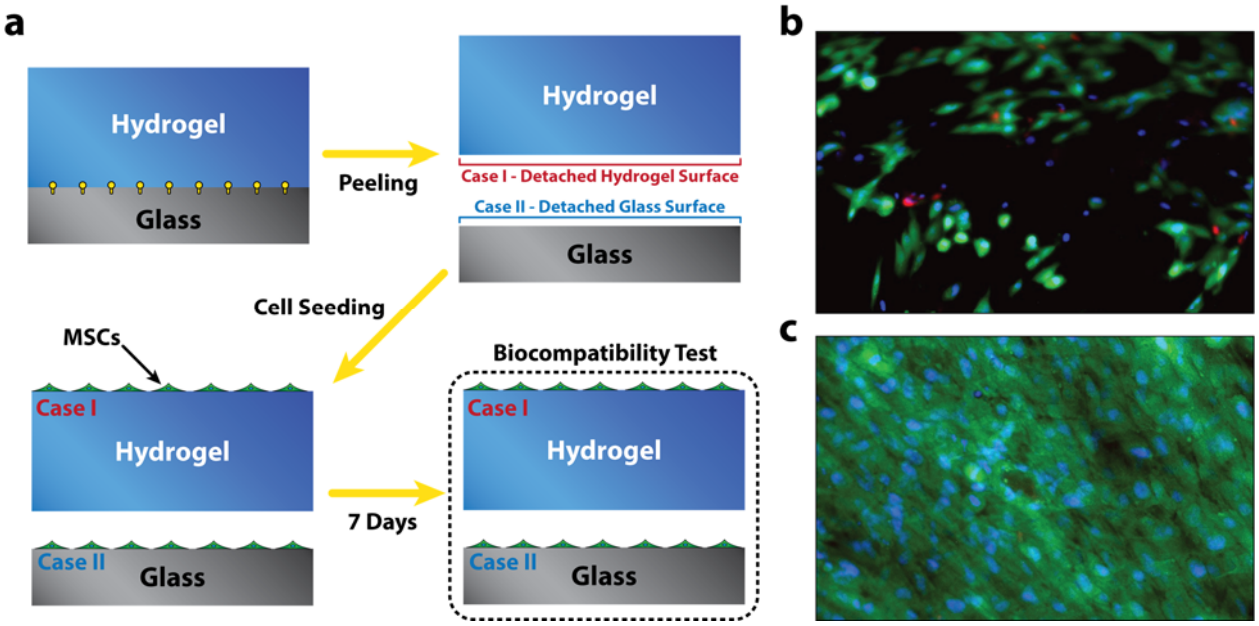

Figure S12. Biocompatibility of PAAm-alginate hydrogel bonded on silane-functionalized glass surface. a. Schematic illustration of the biocompatibility test. The hydrogel was chemically anchored onto the glass slide using TMSPMA. To focus on biocompatibility of hydrogel-solid interface, the hydrogel was peeled off from the glass slide to expose the previously bonded interfaces. The biocompatibility of both exposed interfaces was tested via a live/dead assay of MSCs after seven days of incubation on the exposed interfaces. **b.** The result of live/dead assay of MSCs on the hydrogel. **c.** The result of live/dead assay of MSCs on the glass slide. Note that blue color indicates nuclei of MSCs, green color indicates live MSCs and red color indicates dead MSCs in the live/dead assay. The percentage of viable MSCs on both of the exposed interfaces is over 95 % after seven days of incubation, validating the biocompatibility of the tough bonding.

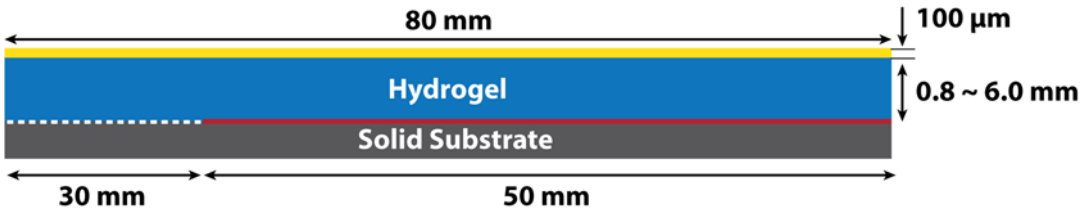

Figure S13. Schematic illustration of the finite-element model for numerical simulation of peeling test. The yellow line indicates the stiff backing and the red line indicates the hydrogel-solid interfacial modeled as a cohesive zone. The white dotted line indicates the unbounded part of hydrogel.

DOI: 10.1038/NMAT4463

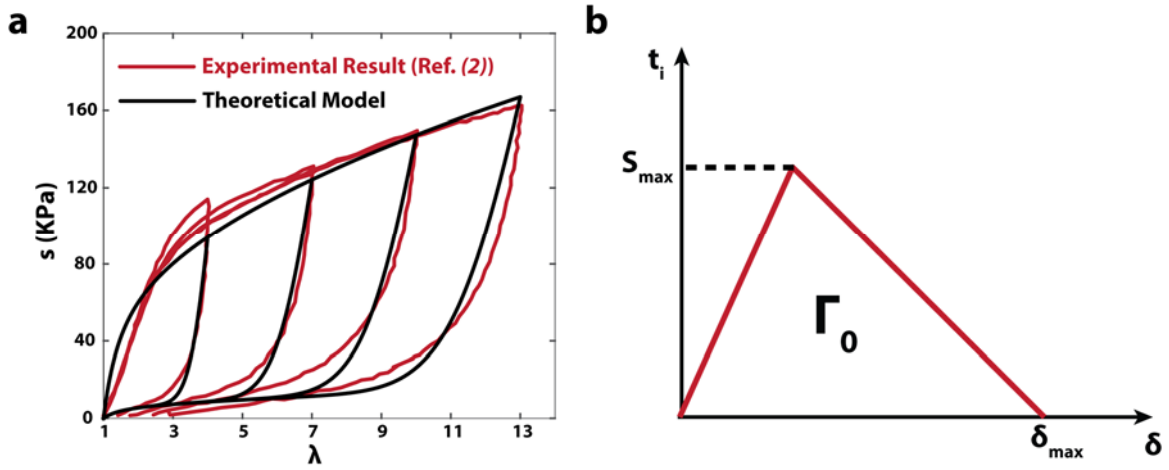

Figure S14. Mullins effect and cohesive-zone model. a. Stress-strain hysteresis of the PAAm-alginate hydrogel measured from experiments and fitted with the Mullins effect model. **b.** Triangular cohesive law for the cohesive layer. $t_i(i = n, s)$ represents the nominal stress, and the subscripts n and s indicate deformation normal to and tangential to the interface, respectively.

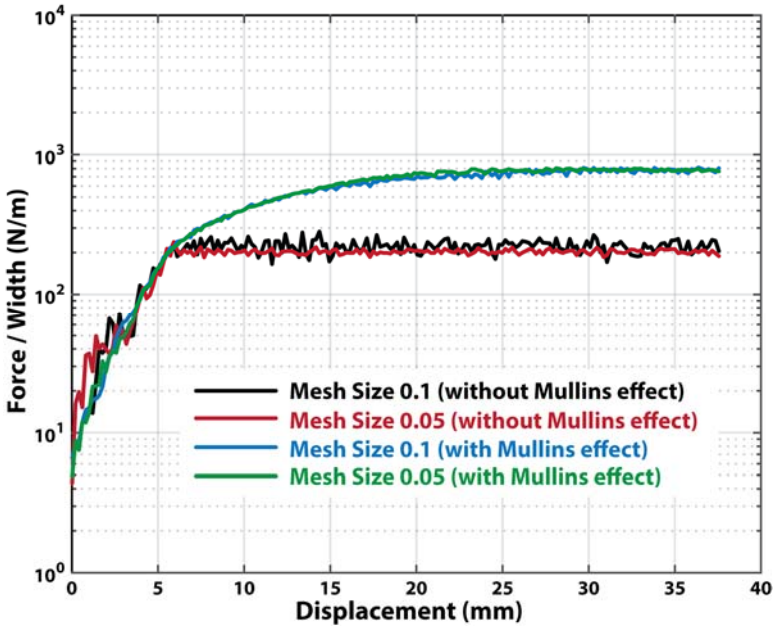

Figure S15. Mesh insensitivity of numerical simulation. Simulation results with fine mesh (0.1) and finer mesh (0.05) showed no difference indicating the mesh insensitivity of the hydrogel peeling simulations.

DOI: 10.1038/NMAT4463

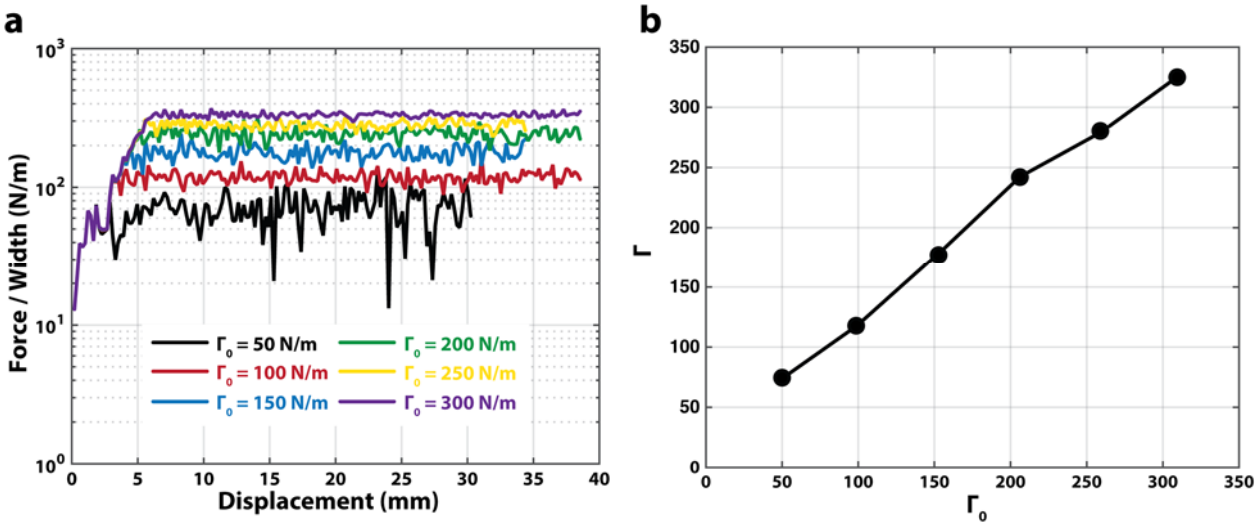

Figure S16. The calculated interfacial toughness Γ of a pure elastic hydrogel bonded on rigid substrates with different intrinsic work of adhesion Γ_0. The hydrogel has otherwise the same mechanical properties as the PAAm-alginate hydrogel. **a.** The calculated curves of peeling force per hydrogel width vs. displacement for bonding with values of Γ_0. **b.** The calculated interfacial toughness as a function of the prescribed Γ_0. The finite-element model gives $\Gamma \approx \Gamma_0$ for pure elastic hydrogel.

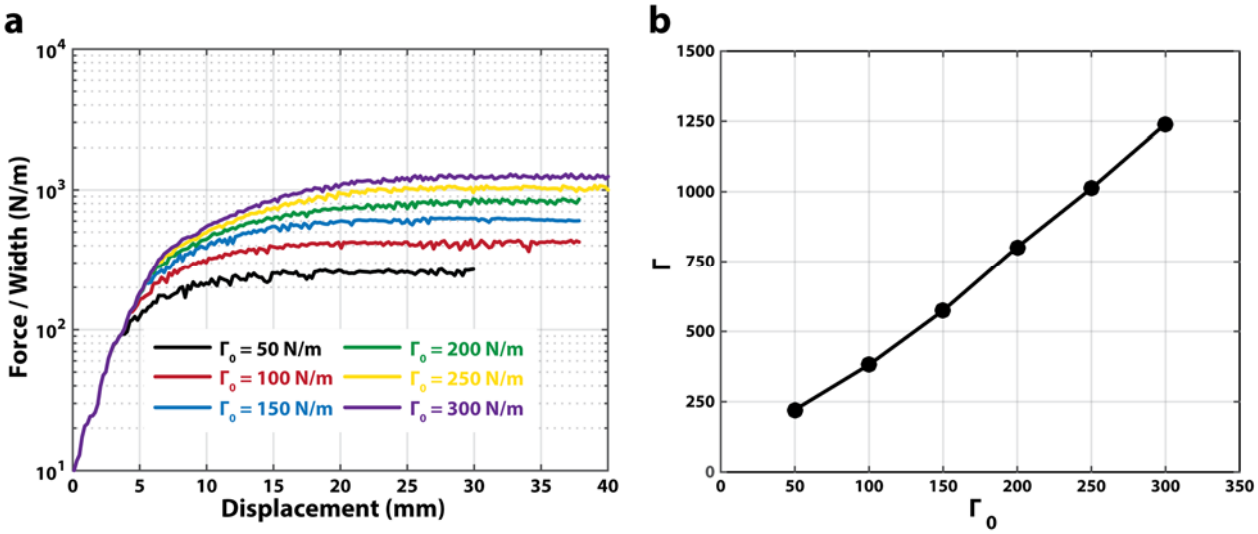

Figure S17. The calculated interfacial toughness Γ of the PAAm-alginate hydrogel bonded on rigid substrates with different intrinsic work of adhesion Γ_0. a. The calculated curves of peeling force per hydrogel width vs. displacement for bonding with different values of Γ_0. **b.** The calculated interfacial toughness as a function of the prescribed Γ_0. The finite-element model shows that the interfacial toughness is multiple times of the intrinsic work of adhesion for PAAm-alginate hydrogel.

DOI: 10.1038/NMAT4463

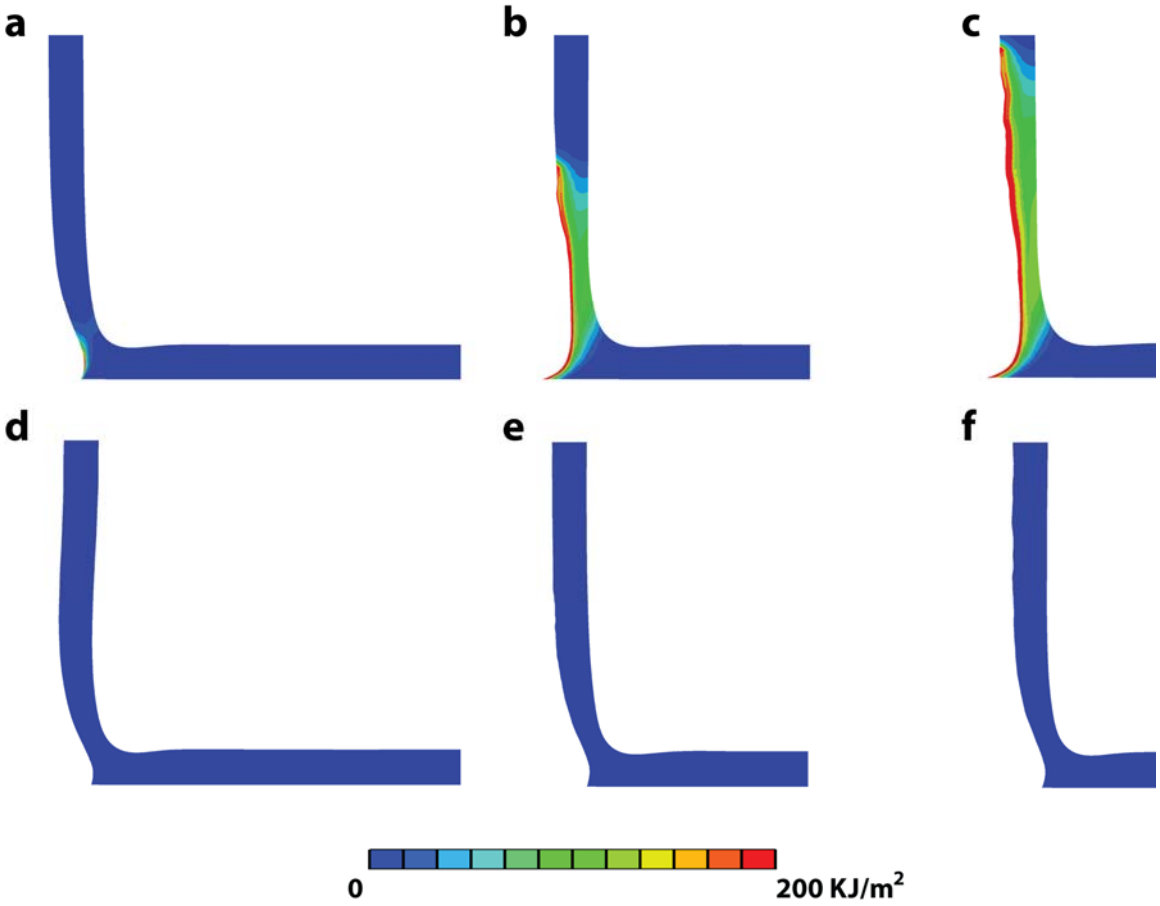

Figure S18. Snapshots of the simulations of the peeling tests. a-c. Peeling process of the PAAm-alginate hydrogel, including crack initiation, crack propagation and stead state. **d-f.** Peeling process of a pure elastic hydrogel, including crack initiation and stead state. The color indicates the energy dissipation per unit area in the materials.

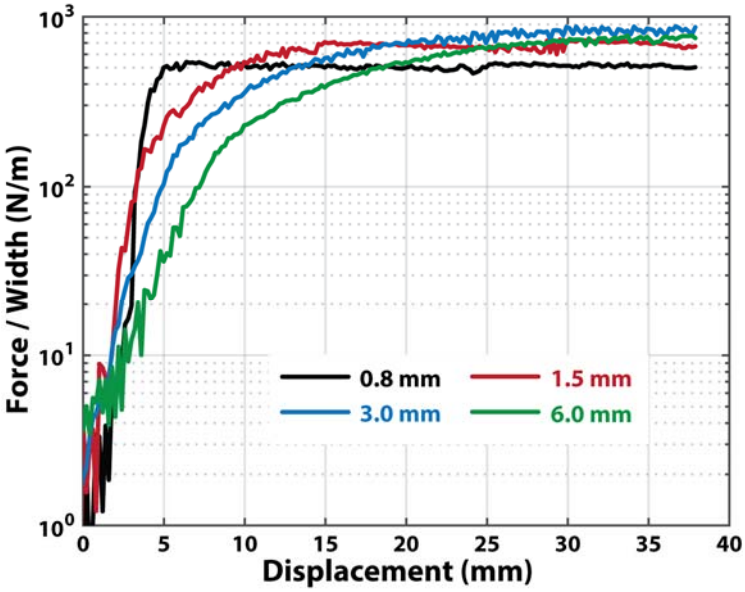

Figure S19. Interfacial toughness of PAAm-alginate hydrogels with different thicknesses bonded on rigid substrates calculated from the finite-element models. The calculated curves of peeling force per hydrogel width vs. displacement for samples with thickness of 0.8 mm, 1.5 mm, 3 mm and 6 mm, respectively. The interfacial toughness does not significantly depend on hydrogel thickness in the range of 1.5 mm – 6 mm.

DOI: 10.1038/NMAT4463

SUPPLEMENTARY MOVIE CAPTIONS

Movie S1: The standard 90-degree peeling test for an as-prepared common hydrogel chemically anchored on glass substrate.

Movie S2: The standard 90-degree peeling test for an as-prepared common or tough hydrogel physically attached on glass substrate.

Movie S3: The standard 90-degree peeling test for an as-prepared tough hydrogel chemically anchored on glass substrate.

Movie S4: The standard 90-degree peeling test for a fully swollen tough hydrogel chemically anchored on titanium substrate.

Movie S5: The process of shattering and consequently deforming a silicon wafer coated with a layer of chemically-anchored tough hydrogel.

Movie S6: Various modes of deformation of four ceramic bars bonded by the flexible and tough hydrogel joints.

Movie S7: An ionic hydrogel chemically anchored on two titanium electrodes is conductive enough to power a LED light even when the hydrogel is under high stretch of 4.5 times, demonstrating that the hydrogel-metal interface is electrically conductive.

Movie S8: Finite-element simulation of the peeling process of the tough hydrogel with energy dissipation (Color indicates energy dissipation per unit area).

Movie S9: Finite-element simulation of the peeling process of a pure elastic hydrogel.

REFERENCES

1 Ogden, R. & Roxburgh, D. A pseudo–elastic model for the Mullins effect in filled rubber. *Proceedings of the Royal Society of London. Series A: Mathematical, Physical and Engineering Sciences* **455**, 2861-2877 (1999).

2 Sun, J.-Y. *et al.* Highly stretchable and tough hydrogels. *Nature* **489**, 133-136 (2012).

3 Kurokawa, T., Furukawa, H., Wang, W., Tanaka, Y. & Gong, J. P. Formation of a strong hydrogel–porous solid interface via the double-network principle. *Acta biomaterialia* **6**, 1353-1359 (2010).

4 Hacking, S., Bobyn, J., Toh, K., Tanzer, M. & Krygier, J. Fibrous tissue ingrowth and attachment to porous tantalum. *Journal of biomedical materials research* **52**, 631-638 (2000).

5 Rose, S. *et al.* Nanoparticle solutions as adhesives for gels and biological tissues. *Nature* **505**, 382-385, doi:10.1038/nature12806 (2014).

6 Bundy, K., Schlegel, U., Rahn, B., Geret, V. & Perren, S. An improved peel test method for measurement of adhesion to biomaterials. *Journal of Materials Science: Materials in Medicine* **11**, 517-521 (2000).

7 Lin, Q. *et al.* Adhesion mechanisms of the mussel foot proteins mfp-1 and mfp-3. *Proceedings of the National Academy of Sciences* **104**, 3782-3786 (2007).

8 Murphy, J. L., Vollenweider, L., Xu, F. & Lee, B. P. Adhesive performance of biomimetic adhesive-coated biologic scaffolds. *Biomacromolecules* **11**, 2976-2984 (2010).

9 Guvendiren, M., Messersmith, P. B. & Shull, K. R. Self-assembly and adhesion of DOPA-modified methacrylic triblock hydrogels. *Biomacromolecules* **9**, 122-128 (2007).

10 Sofla, A., Seker, E., Landers, J. P. & Begley, M. R. PDMS-glass interface adhesion energy determined via comprehensive solutions for thin film bulge/blister tests. *Journal of Applied Mechanics* **77**, 031007 (2010).

11 Shull, K. R., Ahn, D., Chen, W. L., Flanigan, C. M. & Crosby, A. J. Axisymmetric adhesion tests of soft materials. *Macromolecular Chemistry and Physics* **199**, 489-511 (1998).

12 Jang, E.-J. *et al.* Effect of surface treatments on interfacial adhesion energy between UV-curable resist and glass wafer. *International Journal of Adhesion and Adhesives* **29**, 662-669 (2009).

13 Toonder, J. D., Malzbender, J. & Balkenende, R. Fracture toughness and adhesion energy of sol-gel coatings on glass. *Journal of materials research* **17**, 224-233 (2002).

14 Li, L., Tirrell, M., Korba, G. A. & Pocius, A. V. Surface energy and adhesion studies on acrylic pressure sensitive adhesives. *The Journal of Adhesion* **76**, 307-334 (2001).